given in volts. If we accept for the Thomas-Fermi function

$$\Phi(x)=e^{-0.60x}, \tag{22}$$

and we calculate the total cross section Q_0, we obtain the following formula for $Q_0Z^{-\frac{2}{3}}/\pi a_0^2$:

$$\frac{Q_0Z^{-\frac{2}{3}}}{\pi a_0^2}=\frac{75.850}{1+0.7308x^2}. \tag{23}$$

This formula gives for $x>2$ the same results as our formula (21), as is shown in Table II, and thus it may be used for rapid calculation of the total cross section Q_0. Equation (23) corresponds more to a WKB-model for the atom than a Thomas-Fermi model. For x in the range $0\leq x\leq 2$, the results for the total cross section Q_0 given by (21) and (23) differ considerably from each other, since Q_0 given by (21) is infinite for $x=0$ while Q_0 given by (23) is finite for $x=0$.

The authors are indebted to Professor F. J. Wiśniewski for his interest on this paper.

PHYSICAL REVIEW VOLUME 108, NUMBER 2 OCTOBER 15, 1957

Shock-Wave Compressions of Twenty-Seven Metals. Equations of State of Metals*

JOHN M. WALSH, MELVIN H. RICE, ROBERT G. McQUEEN, AND FREDERICK L. YARGER
University of California, Los Alamos Scientific Laboratory, Los Alamos, New Mexico

(Received January 18, 1957)

An explosive system is used to drive a strong shock wave into a plate of 24ST aluminum. This shock wave propagates through the 24ST aluminum into small test specimens which are in contact with the front surface of the plate. A photographic technique is used to measure velocities associated with the 24ST aluminum shock wave and with the shock wave in each specimen.

The measured velocities are transformed, using the conservation relations, to pressure-compression points. Resulting pressure-compression curves are given for 27 metals. The range of data is different for each material but typically covers the pressure interval 150 to 400 kilobars; probable errors in reported experimental pressure-compression curves are 1 or 2% in compression for a given pressure.

The experimental curves, which consist thermodynamically of a known P, V, E locus for each material, are used to calculate a more complete high-pressure equation of state. This is done by means of a theoretical estimate of the volume variation of the Grüneisen ratio $\gamma(V)=V(\partial P/\partial E)_V$. Calculated P, V, T states are listed for the various materials. For 24ST aluminum, quantities of application in shock-wave hydrodynamics are also tabulated.

INTRODUCTION

IN Sec. I an experimental method to obtain dynamic pressure-compression curves for solids is described and resulting data, plotted in Figs. 3–29, are listed for the following 27 solids: beryllium, bismuth, cadmium, chromium, cobalt, copper, gold, iron, lead, magnesium, molybdenum, nickel, silver, thorium, tin, titanium, zinc, 24ST aluminum, brass, indium, niobium, palladium, platinum, rhodium, tantalum, thallium, and zirconium.

Section II is devoted to the problem of generalizing the experimental Hugoniot curves into a complete thermodynamic description of high pressure states neighboring the experimental curves.

Throughout the present discussion it is assumed that stresses behind the shock wave are isotropic, and that the compressed materials behind the shock wave are in thermodynamic equilibrium. Further discussion of basic principles underlying the present work is found in previous papers[1,2] dealing with dynamic pressure-compression results.

I. DETERMINATION OF HUGONIOT CURVES

A. Measurement of Shock Wave and Free-Surface Velocities

The experimental method used to measure shock wave and free-surface velocities is illustrated in Fig. 1. The detonation of the explosive system, pictured at the top of the figure, causes a plane shock wave to be transmitted into the 24ST aluminum plate. This shock wave next interacts with the test specimen, Lucite, iron-shim assembly on the front surface of the plate. The essential features of this assembly are the two rows of test pellets and the 0.003-in. thick argon-filled flash gaps. The pellets consist of one row of five thick specimens (0.250 in. thick by 0.750 in. diameter) to provide for shock velocity measurements and one row of thin specimens (0.125 in. thick by 0.750 in. diameter) for

* Work done under the auspices of the U. S. Atomic Energy Commission.

[1] J. M. Walsh and R. H. Christian, Phys. Rev. **97**, 1544 (1955).
[2] Goranson, Bancroft, Burton, Blechar, Houston, Gittings, and Landeen, J. Appl. Phys. **26**, 1472 (1955).

free-surface velocity measurements of the same five materials. The flash gaps, when closed by the shock wave, provide light (due to multiple shock reflections in the argon) which is recorded by a moving image camera. The camera, in an underground bunker some 15 feet from the shot assembly, views the assembly through a slit system and sweeps the image in a direction normal to the slits.

A photographic record is also seen in Fig. 1, where

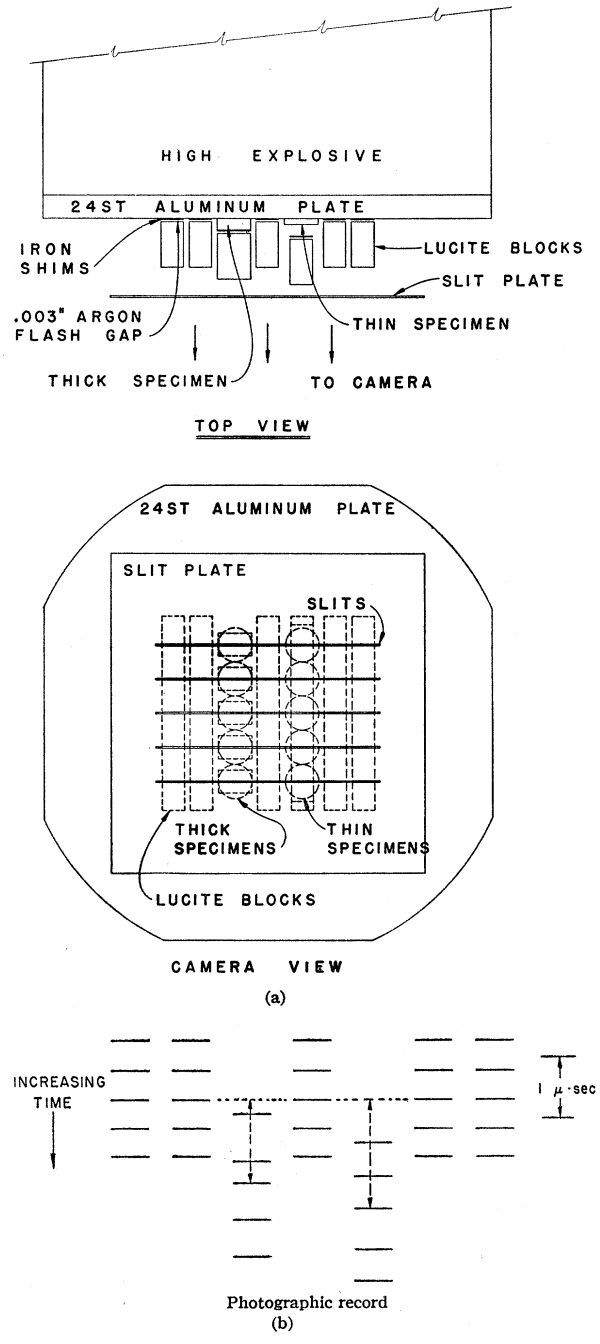

FIG. 1. Drawing of sweep camera photographic record.

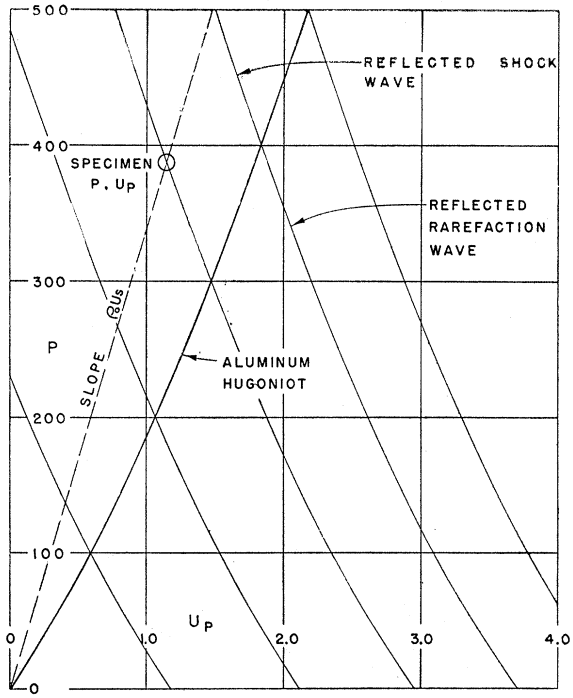

FIG. 2. Pressure *versus* particle velocity curves for 24ST aluminum, and a typical graphical solution to determine P, U_p for a test specimen.

pertinent features are identified. The record is analyzed by comparator reading, measured record offsets being converted to times by use of the known camera sweep speed. The measured time[3] offset for the thick pellet is divided into pellet thickness to give the shock wave velocity for that material. The measured time for the thin pellet of the same material is the shock wave transit time through the thin pellet plus the time required for the free surface to traverse the free-run distance. When combined with the measured shock wave velocity and the known free-run distance, it gives the desired free-surface velocity. The measured shock wave and free-surface velocities are listed in Table I, second and third columns.

B. Transformation of Measured Velocities to Pressure-Volume Points

The transformation of measured velocities to pressure-compression points is done by two methods, both of

[3] Small corrections are incorporated into the measured time offsets. These corrections arise from the fact that the 0.003-in. argon flash gaps over test specimen are closed at different velocities from the flash gaps over the main 24ST aluminum plate. The magnitude of each correction is determined by solution of the appropriate interface problems, using the graphical pressure-particle velocity method discussed below. The applied corrections are taken to be the total difference in flash-gap closure times from the assumption that the light flash occurs in the final stages of closure of the flash gap. The corrections seldom affect measured velocities more than 0.5%, and more typically cause a change of about 0.2%.

TABLE I. Experimental data.

Metal	Shock wave velocity U_s (km/sec)	Free surface velocity U_{fs} (km/sec)	Free surface approximation: Pressure P (kilobars)	Free surface approximation: Relative volume V/V_0	Graphical solution: Shock particle velocity U_p (km/sec)	Graphical solution: Pressure P (kilobars)	Graphical solution: Relative volume V/V_0
Beryllium	9.044	1.697	141.6	0.9062	0.847	141.3	0.9063
$\rho_0=1.845$ g/cm³	8.934	1.739	143.3	0.9027	0.865	142.6	0.9032
$C_p=0.474$ cal/g °C	9.112	2.358	198.2	0.8706	1.189	199.9	0.8695
$\frac{1}{V}\left(\frac{\partial V}{\partial T}\right)_p=37\times10^{-6}$/°C	9.332	2.364	203.5	0.8733	1.221	210.2	0.8692
	9.851	3.422	311.0	0.8263	1.730	314.4	0.8244
	9.832	3.235	293.4	0.8355	1.609	291.9	0.8364
	9.633	3.189	283.4	0.8345	1.592	282.9	0.8347
Bismuth	2.696	1.401	184.9	0.7402	0.718	189.5	0.7337
$\rho_0=9.79$ g/cm³	2.585	1.318	166.8	0.7451	0.676	171.1	0.7385
$C_p=0.293$ cal/g °C	3.075	1.793	269.9	0.7085	0.914	275.2	0.7028
$\frac{1}{V}\left(\frac{\partial V}{\partial T}\right)_p=40\times10^{-6}$/°C	3.084	1.800	271.7	0.7082	0.922	278.4	0.7010
	3.682	2.476	446.3	0.6638	1.212	436.9	0.6708
	3.659	2.564	459.2	0.6496	1.222	437.7	0.6660
Cadmium	3.599	1.464	227.5	0.7966	0.690	214.4	0.8083
$\rho_0=8.64$ g/cm³	3.421	1.277	188.6	0.8134	0.619	182.9	0.8191
$C_p=0.055$ cal/g °C	3.918	1.757	297.2	0.7758	0.850	287.6	0.7830
$\frac{1}{V}\left(\frac{\partial V}{\partial T}\right)_p=89.4\times10^{-6}$/°C	4.450	2.496	479.6	0.7196	1.190	457.3	0.7326
	4.324	2.400	448.1	0.7225	1.120	418.2	0.7410
Chromium	6.043				0.5448	234.5	0.9098
$\rho_0=7.13$	5.923				0.5395	233	0.9089
$C_p=0.065$	6.381				0.7436	338	0.8835
$\frac{1}{V}\left(\frac{\partial V}{\partial T}\right)_p=18.6\times10^{-6}$/°C	6.370				0.7449	338	0.8831
	6.355				0.7407	336	0.8834
	6.357				0.7403	336	0.8835
	6.660				1.007	478	0.8488
	6.674				1.008	479	0.8490
Cobalt	5.445	1.016	244.0	0.9067	0.502	241.1	0.9078
$\rho_0=8.82$	5.696	1.327	333.4	0.8835	0.683	343.2	0.8801
$C_p=0.099$	5.632	1.334	331.4	0.8816	0.653	324.4	0.8841
$\frac{1}{V}\left(\frac{\partial V}{\partial T}\right)_p=36.9\times10^{-6}$/°C	6.019	...	...	...	0.901	478.1	0.8503
	6.052	1.890	504.5	0.8439	0.955	509.8	0.8422
Copper	4.744	1.024	216.2	0.8921	0.511	215.8	0.8923
$\rho_0=8.90$	4.768	1.094	232.1	0.8853	0.570	241.9	0.8804
$C_p=0.092$	5.070	1.440	324.9	0.8580	0.711	320.8	0.8598
$\frac{1}{V}\left(\frac{\partial V}{\partial T}\right)_p=49.5\times10^{-6}$/°C	5.015	1.456	324.9	0.8548	0.731	326.3	0.8542
	5.508	2.079	509.6	0.8113	1.032	505.9	0.8126
Gold	3.679	0.771	272.9	0.8952	0.380	269.0	0.8967
$\rho_0=19.24$	3.864	1.012	376.2	0.8690	0.505	375.4	0.8693
$C_p=0.312$	4.130	1.375	546.3	0.8335	0.666	529.2	0.8389
$\frac{1}{V}\left(\frac{\partial V}{\partial T}\right)_p=42.6\times10^{-6}$/°C							
Iron	5.652	2.163	479.2	0.8087	1.085	480.8	0.8080
$\rho_0=7.84$	5.474	2.037	437.1	0.8139	1.013	434.7	0.8149
$C_p=0.107$	5.458	1.988	425.3	0.8179	0.993	424.9	0.8181
$\frac{1}{V}\left(\frac{\partial V}{\partial T}\right)_p=35.1\times10^{-6}$/°C	5.438	2.005	427.4	0.8156	0.994	423.8	0.8172
	5.229	1.789	366.7	0.8289	...	...	...
	5.231	1.773	363.6	0.8305	...	...	...
	5.206	1.755	358.2	0.8314	...	...	...
	5.209	1.755	358.4	0.8315	...	...	...
Lead	2.914	1.230	203.0	0.7889	0.590	194.8	0.7975
$\rho_0=11.34$	3.268	1.745	323.1	0.7330	0.819	303.2	0.7494
$C_p=0.030$	3.250	1.731	318.7	0.7337	0.802	295.3	0.7532
$\frac{1}{V}\left(\frac{\partial V}{\partial T}\right)_p=85.1\times10^{-6}$/°C	3.724	2.420	510.5	0.6751	1.118	471.7	0.6998
Magnesium	5.987	2.242	116.4	0.8128			
$\rho_0=1.735$	7.082	4.157	260.4	0.7066			
$C_p=0.250$							
$\frac{1}{V}\left(\frac{\partial V}{\partial T}\right)_p=76.8\times10^{-6}$/°C							

TABLE I.—*Continued.*

Metal	Shock wave velocity U_s (km/sec)	Free surface velocity U_{fs} (km/sec)	Free surface approximation: Pressure P (kilobars)	Free surface approximation: Relative volume V/V_0	Graphical solution: Shock particle velocity U_p (km/sec)	Graphical solution: Pressure P (kilobars)	Graphical solution: Relative volume V/V_0
Molybdenum	5.699	0.874	254.0	0.9233	0.437	254.0	0.9233
$\rho_0=10.20$	5.647	0.888	255.7	0.9214	0.444	255.2	0.9214
$C_p=0.0612$	5.955	1.176	357.2	0.9013	0.591	359.0	0.9008
$\frac{1}{V}\left(\frac{\partial V}{\partial T}\right)_p=15\times10^{-6}/°C$	5.861	1.200	358.7	0.8976	0.606	362.3	0.8966
	6.210	1.724	546.0	0.8612	0.850	538.4	0.8631
	6.124	1.636	511.0	0.8664	0.792	494.7	0.8707
Nickel	5.417	0.981	235.3	0.9095	0.490	235.0	0.9095
$\rho_0=8.86$	5.653	1.350	337.8	0.8806	0.678	339.4	0.8801
$C_p=0.1050$	5.620	1.390	345.8	0.8763	0.687	341.8	0.8778
$\frac{1}{V}\left(\frac{\partial V}{\partial T}\right)_p=39\times10^{-6}/°C$	6.031	1.955	522.0	0.8379	0.957	511.0	0.8413
	5.969	1.981	523.5	0.8341	0.982	519.0	0.8355
	5.952	1.835	483.5	0.8459	0.887	467.4	0.8510
Silver	4.065	1.015	216.4	0.8752	0.504	214.9	0.8760
$\rho_0=10.49$	4.113	1.049	226.3	0.8725	0.527	227.4	0.8719
$C_p=0.056$	4.378	1.448	332.5	0.8346	0.717	329.3	0.8362
$\frac{1}{V}\left(\frac{\partial V}{\partial T}\right)_p=56.7\times10^{-6}/°C$	4.846	2.041	518.8	0.7894	0.985	500.7	0.7967
	4.848	2.074	527.4	0.7861	1.010	513.6	0.7917
Thorium	3.497	2.112	431.3	0.6980	1.043	426.0	0.7017
$\rho_0=11.68$	3.192	1.604	299.0	0.7487	0.812	302.7	0.7456
$C_p=0.030$	2.954	1.246	215.0	0.7891	0.620	213.9	0.7901
$\frac{1}{V}\left(\frac{\partial V}{\partial T}\right)_p=33.3\times10^{-6}/°C$	2.900	1.198	202.9	0.7934	0.571	193.4	0.8031
Tin	4.555	2.704	448.3	0.7032	1.290	427.8	0.7168
$\rho_0=7.28$	4.435	2.539	409.9	0.7138	1.190	384.2	0.7317
$C_p=0.054$	4.004	1.912	278.7	0.7612	0.925	269.6	0.7690
$\frac{1}{V}\left(\frac{\partial V}{\partial T}\right)_p=60\times10^{-6}/°C$	3.557	1.486	192.4	0.7911	0.705	182.6	0.8018
	3.524	1.364	175.0	0.8065	0.670	171.9	0.8098
Titanium	6.329	2.723	388.1	0.7849	1.370	390.8	0.7835
$\rho_0=4.51$	5.790	1.926	251.3	0.8337	0.980	255.7	0.8307
$C_p=0.126$	5.501	1.437	178.1	0.8694	0.723	179.3	0.8686
$\frac{1}{V}\left(\frac{\partial V}{\partial T}\right)_p=25.5\times10^{-6}/°C$	5.469	1.364	168.1	0.8753	0.684	168.6	0.8749
Zinc	5.014	2.589	463.1	0.7418	1.250	447	0.7507
$\rho_0=7.135$	4.870	Zinc single-crystal experiment. See Sec. I-D			1.190	414	0.7556
$C_p=0.092$	4.481	1.795	286.9	0.7997	0.88	281.4	0.8036
$\frac{1}{V}\left(\frac{\partial V}{\partial T}\right)_p=100\times10^{-6}/°C$	4.450	1.826	289.9	0.7948	0.894	283.9	0.7991
	4.465	1.823	290.4	0.7959			
	4.053	1.355	195.9	0.8328	0.650	188.0	0.8396
	4.059	1.345	194.8	0.8343			
	4.13	Zinc single-crystal experiment. See Sec. I-D			0.673	198.3	0.8370
	4.022	1.295	185.8	0.8390	0.630	180.8	0.8434
	4.029	1.310	188.3	0.8374			
24ST aluminum	7.531	3.230	335.8	0.7874			
$\rho_0=2.785$	6.927	2.319	222.7	0.8333			
$C_p=0.23$	6.500	1.700	153.5	0.8696			
$\frac{1}{V}\left(\frac{\partial V}{\partial T}\right)_p=69.0\times10^{-6}/°C$	Actual 24ST aluminum data consists of approximately one-hundred points of which the above three are representative.						
Brass	4.446	1.181	220.9	0.8672	0.590	220.7	0.8673
$\rho_0=8.413$	4.440	1.143	213.5	0.8713	0.571	213.3	0.8714
$C_p=0.09$	4.731	1.553	309.1	0.8359	0.791	314.8	0.8328
$\frac{1}{V}\left(\frac{\partial V}{\partial T}\right)_p=61.6\times10^{-6}/°C$	4.726	1.569	311.9	0.8340	0.770	306.2	0.8371
	5.236	2.200	484.6	0.7899	1.085	478.0	0.7928
	5.220	...	...	...	1.077	473.0	0.7937
Indium	3.745				0.7837	213.5	0.7907
$\rho_0=7.27$	3.965				0.9812	283	0.7525
$C_p=0.057$	4.348				1.281	405	0.7054
$\frac{1}{V}\left(\frac{\partial V}{\partial T}\right)_p=99\times10^{-6}/°C$							

TABLE I.—*Continued.*

Metal	Shock wave velocity U_s (km/sec)	Free surface velocity U_{fs} (km/sec)	Free surface approximation: Pressure P (kilobars)	Free surface approximation: Relative volume V/V_0	Graphical solution: Shock particle velocity U_p (km/sec)	Graphical solution: Pressure P (kilobars)	Graphical solution: Relative volume V/V_0
Niobium	5.177				0.5489	244.5	0.8940
$\rho_0=8.604$	5.311				0.7434	341	0.8606
$C_p=0.065$	5.642				0.9929	482	0.8240
$\frac{1}{V}\left(\frac{\partial V}{\partial T}\right)_p=23.3\times10^{-6}/°C$							
Palladium	4.673				0.4728	262.5	0.8988
$\rho_0=11.95$	5.004				0.6200	372	0.8761
$C_p=0.0583$	5.374				0.8219	531	0.8471
$\frac{1}{V}\left(\frac{\partial V}{\partial T}\right)_p=35\times10^{-6}/°C$							
Platinum	4.199				0.329	295	0.9238
$\rho_0=21.37$	4.306				0.4550	416.5	0.8943
$C_p=0.0322$	4.495				0.6102	586	0.8642
$\frac{1}{V}\left(\frac{\partial V}{\partial T}\right)_p=26.7\times10^{-6}/°C$							
Rhodium	5.470				0.4100	278.5	0.9250
$\rho_0=12.42$	5.865				0.7566	551	0.8710
$C_p=0.059$							
$\frac{1}{V}\left(\frac{\partial V}{\partial T}\right)_p=25\times10^{-6}/°C$							
Tantalum	3.811				0.4327	271.5	0.8865
$\rho_0=16.46$	4.010				0.5800	383	0.8554
$C_p=0.034$	4.323				0.7685	547	0.8222
$\frac{1}{V}\left(\frac{\partial V}{\partial T}\right)_p=19.5\times10^{-6}/°C$							
Thallium	2.804				0.6416	213	0.7712
$\rho_0=11.84$	2.817				0.6386	213	0.7733
$C_p=0.031$	3.120				0.8446	312	0.7293
	3.145				0.8406	313	0.7327
$\frac{1}{V}\left(\frac{\partial V}{\partial T}\right)_p=114\times10^{-6}/°C$	3.538				1.090	456.5	0.6919
	3.541				1.089	456.5	0.6925
Zirconium	4.494				0.7117	207.5	0.8416
$\rho_0=6.49$	4.674				0.9563	290	0.7954
$C_p=0.068$	4.920				1.275	407	0.7408
$\frac{1}{V}\left(\frac{\partial V}{\partial T}\right)_p=15.6\times10^{-6}/°C$							

which use the Rankine-Hugoniot relations

$$V/V_{0H}=(U_s-U_p)/U_s, \tag{1}$$

$$P_H=\rho_0 U_s U_p+P_{0H}, \tag{2}$$

for the conservations of mass and momentum across a shock front. Here P_{0H}, V_{0H} refer to pressure and specific volume for the undisturbed state ahead of the shock front and P_H, V denote pressure and specific volume for the state behind the shock front. U_s and U_p are, respectively, the shock wave velocity, and the particle velocity for the state behind the shock front, each relative to the undisturbed state ahead of the shock front.

For the first transformation method, we note that the experimental free-surface velocity, U_{fs}, is the sum of the shock particle velocity and the particle velocity, U_r, due to the centered rarefaction wave which relieves the pressure, i.e.,

$$U_{fs}=U_p+U_r. \tag{3}$$

The approximate relation[4] $U_r/U_p\approx1$, or equivalently

$$U_p\approx U_{fs}/2, \tag{4}$$

is combined with Eqs. (1), (2), and measured values of U_s and U_{fs} to determine pressure-volume points. Resulting data are listed in Table I under *Free Surface Approximation* and are plotted in Figs 3–29 as ×'s.

[4] Calculated refinements of the free-surface velocity approximation are discussed in Sec. II-B and listed in Table VII. The approximation was also discussed in reference 1, where expressions for possible errors associated with its use were shown to be small.

The second transformation method makes use of certain equation of state data for 24ST aluminum. The necessary 24ST aluminum data (derived using experimental 24ST aluminum results in the next section of this paper) are the curves of pressure *versus* particle velocity shown in Fig. 2. The curve from the origin is the locus of all pressure-particle velocity states attainable by propagating a right-going shock wave into normal undisturbed 24ST aluminum at $P=0$, $U_p=0$. When such a shock wave interacts with the 24ST aluminum-specimen interface, a left-going disturbance is reflected into the aluminum. The locus of P, U_p states that can be reached by the reflected disturbance is given by the appropriate cross curve in Fig. 2. For pressures greater (and particle velocities smaller) than that corresponding to the initial right-going shock wave, the cross curve corresponds to reflected shock waves. For smaller pressures (and greater particle velocities) the cross curve corresponds to a rarefaction wave which is reflected leftward from the interface. The $P=0$ point on each cross curve, in particular, corresponds to the aluminum free-surface velocity for that shock strength.

For the procedure below, it is necessary to identify the cross curve corresponding to the shock wave in the 24ST aluminum plate. This information is obtained by including a pair of 24ST pellets among the test specimens in each shot. The measured free-surface velocity then identifies the desired cross curve from its intercept with the particle velocity axis. Similarly, the measured shock wave velocity is used to construct a line from the origin in Fig. 2 of slope $\rho_0 U_s$ whose intercept with the above-described locus of right-going shocks determines [see Eq. (1) for $P_0 \approx 0$] the (P,U_p) point for the aluminum shock wave, and consequently determines the associated cross curve. The two determinations of the cross curve are averaged to give the value used in the succeeding analysis.

The boundary conditions that pressure and particle velocity must be continuous across the interface between the 24ST aluminum and the test specimen can now be used to construct a graphical solution. First, the known initial density ρ_0 and the measured shock velocity U_s for each specimen are used to construct a line from the origin (see Fig. 3) of slope $\rho_0 U_s$. From Eq. (1), for $P_0 \approx 0$, it is seen that the desired (P,U_p) point for the shock lies on this ray. The intersection of this ray with the aluminum cross curve then satisfies the boundary conditions and gives the desired pressure and particle velocity. The associated relative volume is then calculated by substituting this particle velocity and the measured shock velocity, U_s, into Eq. (2). Pressure-volume points determined by this method are listed under *Graphical Solutions* in Table I and are plotted in Figs. 3–29 as circles.

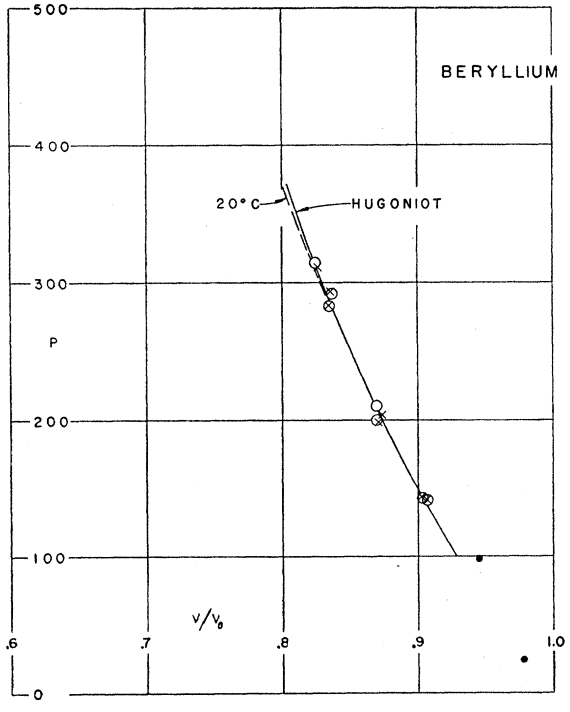

FIG. 3. Pressure-compression curves for beryllium. The solid curve in this figure and in Figs. 4 to 29 is an analytical fit (Table II) of Hugoniot curve experimental data obtained by the graphical solution method. Points plotted as circles in these figures are from the graphical solution method; points plotted as X's are from the free-surface approximation method. (See Sec. IB.) The dashed curve in each figure is a 20°C isotherm, computed using the Hugoniot curve and the methods given in Sec. II. Data points below 100 kilobars are from recent articles by P. W. Bridgman.

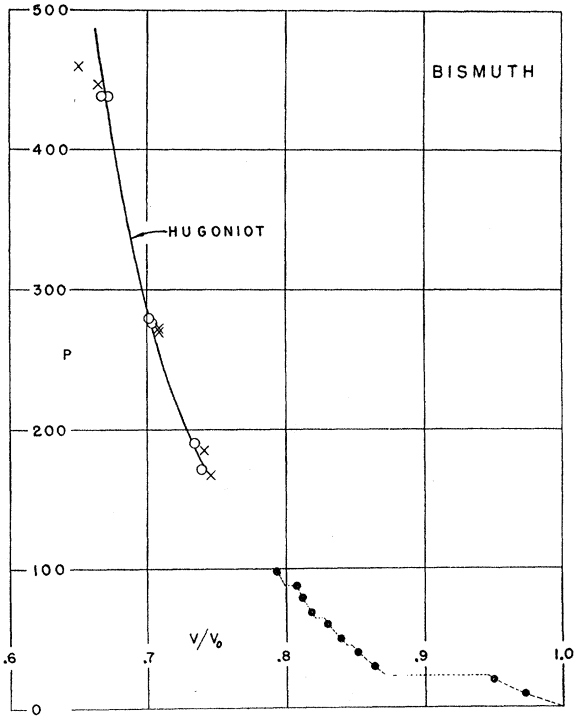

FIG. 4. Pressure-compression curves for bismuth. See caption to Fig. 3.

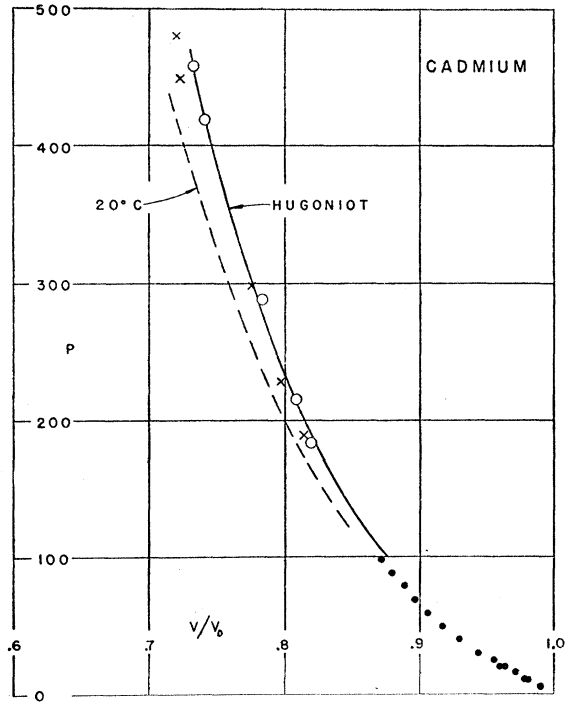

FIG. 5. Pressure-compression curves for cadmium. See caption to Fig. 3.

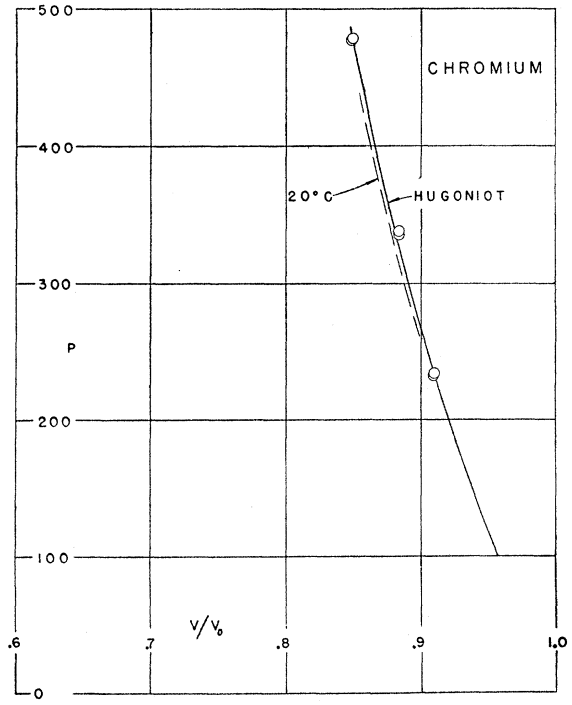

FIG. 6. Pressure-compression curves for chromium. See caption to Fig. 3.

A few of the experiments reported in Table I were done without free-surface velocity measurements, so that only graphical solutions are listed. Iron and magnesium experiments were performed without 24ST aluminum backer plates, so that only free-surface approximation solutions are reported.

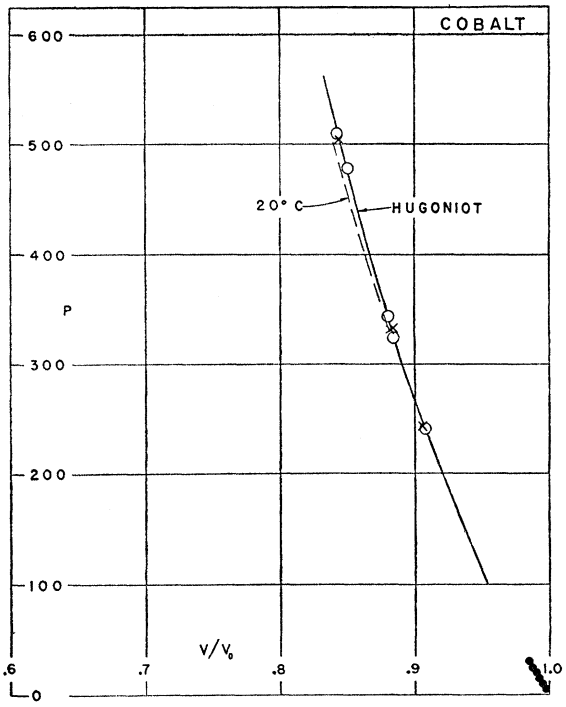

FIG. 7. Pressure-compression curves for cobalt. See caption to Fig. 3.

C. Analytical Fits of Pressure-Volume Data

The Hugoniot curves which are drawn through the experimental points in Figs. 3–29 are reproduced by analytical fits of the form

$$P_H = A\mu + B\mu^2 + C\mu^3, \tag{5}$$

where

$$\mu \equiv (\rho/\rho_0) - 1 = (V_{0H}/V) - 1.$$

The values of A, B, and C for the various solids are listed in Table II. In reality this is a two-parameter fit, since the ratio B/A is determined theoretically by a method given in Sec. II. The two remaining parameters are then selected to fit the results of the present high-pressure experiments. This procedure, as seen by inspection of the figures, gives a satisfactory fit of the present data, and it also forms a standardized extrapolation procedure from which rough comparisons will be made with the lower pressure data from static experimentation.

Finally, from the third mechanical conservation relation

$$E_H - E_{0H} = \tfrac{1}{2}(P_H + P_{0H})(V_{0H} - V), \tag{6}$$

it is seen that the specific internal energy E_H relative

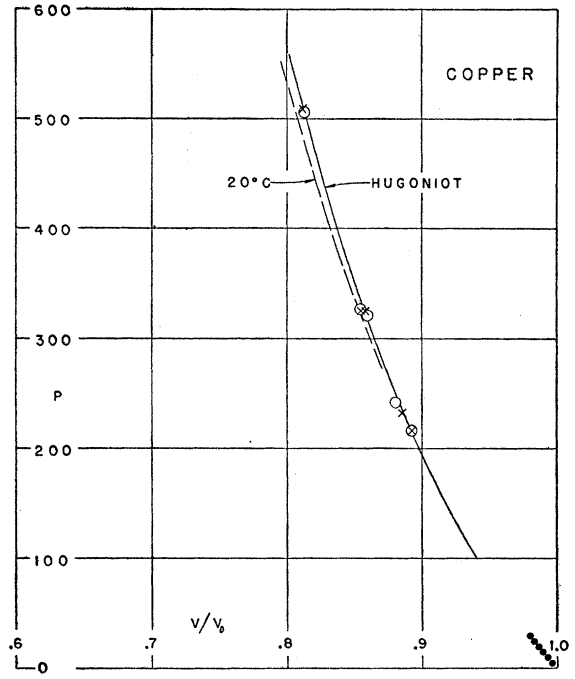

FIG. 8. Pressure-compression curves for copper. See caption to Fig. 3.

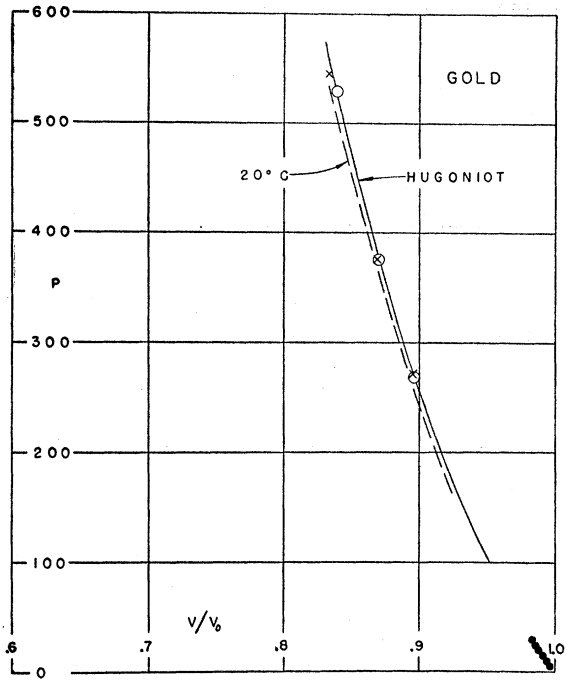

FIG. 9. Pressure-compression curves for gold. See caption to Fig. 3.

to the initial energy E_{0H} can be written (since $P_{0H} \doteq 0$)

$$E_H - E_{0H} = (A\mu^2 + B\mu^3 + C\mu^4)/[2\rho_0(\mu+1)]. \quad (7)$$

Equations (5), (7), and Table II summarize all the experimental thermodynamic information which are available from the shock-wave measurements.

TABLE II. Analytical fits of Hugoniot curves, $P = A\mu + B\mu^2 + C\mu^3$, with pressure in kilobars.

Metal	A	B	C
Beryllium	1182	1382	0
Cadmium	479	1087	2829
Chromium	2070	2236	7029
Cobalt	1954	3889	1728
Copper	1407	2871	2335
Gold	1727	5267	0
Lead	417	1159	1010
Magnesium	370	540	186
Molybdenum	2686	4243	733
Nickel	1963	3750	0
Silver	1088	2687	2520
Thorium	572	646	855
Tin	432	878	1935
Titanium	990	1168	1246
Zinc	662	1577	1242
24ST aluminum	765	1659	428
Brass	1037	2177	3275
Indium	496	1163	0
Niobium	1658	2786	0
Palladium	1744	3801	15 230
Platinum	2760	7260	0
Rhodium	2842	6452	0
Tantalum	1790	3023	0
Thallium	317	938	1485
Zirconium	934	720	0

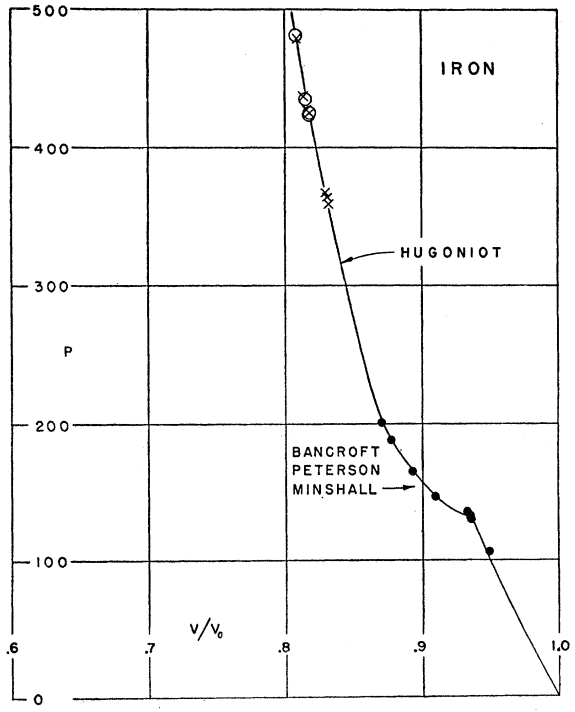

FIG. 10. Pressure-compression curves for iron. See caption to Fig. 3.

D. Zinc Single-Crystal Experiments

Two experiments with zinc single crystals were performed to determine whether observed compressions

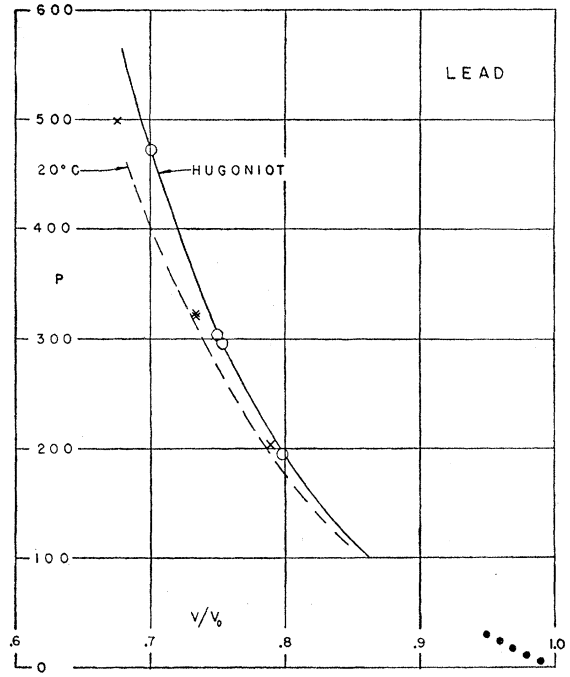

FIG. 11. Pressure-compression curves for lead. See caption to Fig. 3.

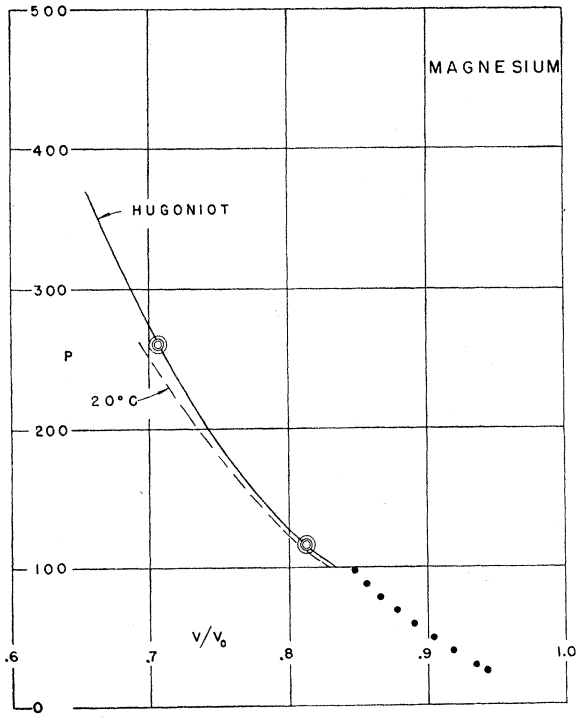

FIG. 12. Pressure-compression curves for magnesium. See caption to Fig. 3.

were dependent upon the crystal orientation. Three zinc crystals of known orientation (shock propagation directions along the C axis, along an A axis, and midway between two A axes) were used in each shot. Shock velocity was measured for each crystal and shock strength was measured for the 24ST aluminum driver plate. The measured values were then used to determine pressure-volume points by the graphical solution method.

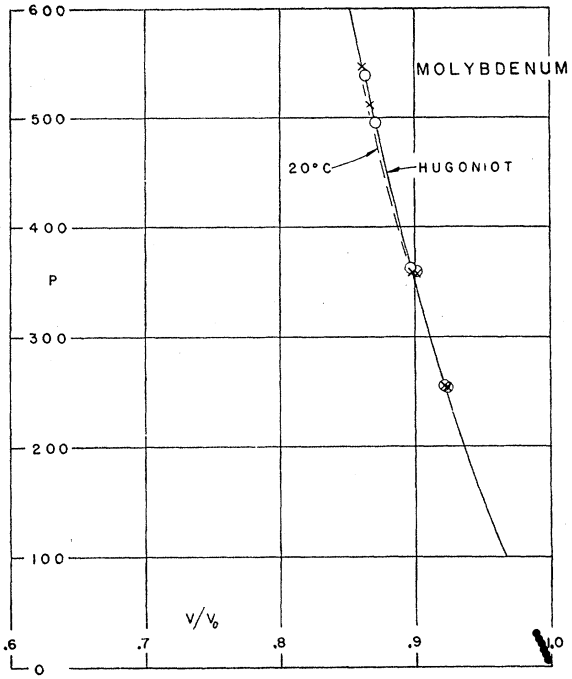

FIG. 13. Pressure-compression curves for molybdenum. See caption to Fig. 3.

The total spread for the three zinc shock velocities in the high-pressure (414 kilobars) shot was 1%, and the corresponding spread for the low-pressure (200 kilobars) shot was 1.5%. Comparable scatters would be expected even if identical specimens were measured so that, within experimental error, one must conclude that results show no dependence of shock velocity (hence compressibility) upon crystallographic orientation. The measured shock velocities from each shot were averaged to obtain the value used in the graphical solutions. The data are listed under zinc in Table I and are also plotted in Fig. 19, where they exhibit good agreement with results obtained using ordinary cast polycrystalline zinc.

The shock wave results differ from the lower pressure static measurements[5] which indicate a several-fold difference in compressibility depending upon whether the compression is parallel to the C axis or normal to it.

E. Discussion of Experimental Data

The probable error per data point, determined from the observed reproducibility, is 0.7% in shock velocity for a given free-surface velocity (about 1% in compression, $1-V/V_0$, at a given pressure). This estimate

[5] P. W. Bridgman, Proc. Am. Acad. Arts Sci. 77, 189 (1949).

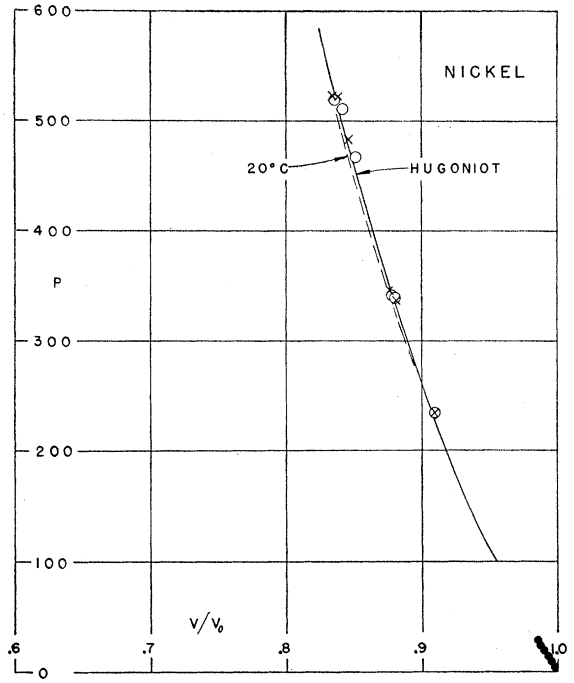

FIG. 14. Pressure-compression curves for nickel. See caption to Fig. 3.

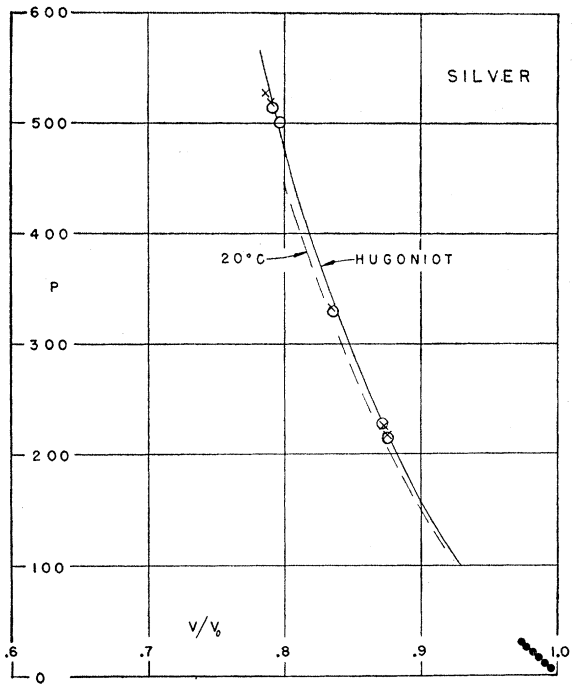

FIG. 15. Pressure-compression curves for silver. See caption to Fig. 3.

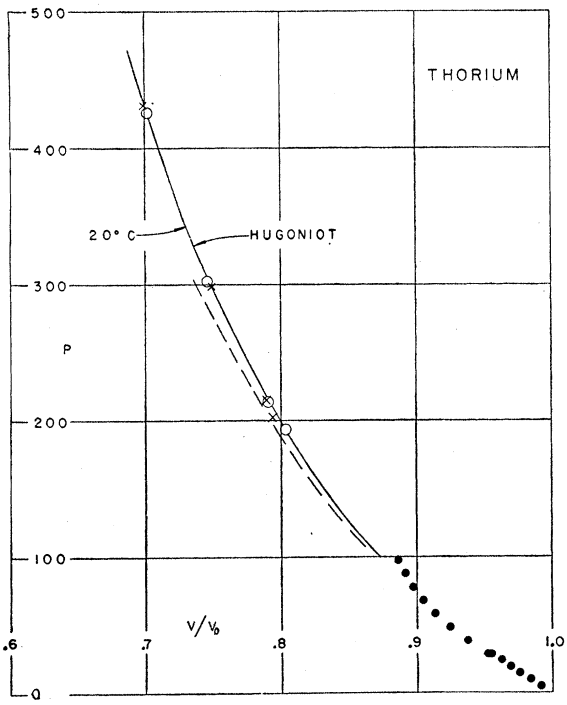

FIG. 16. Pressure-compression curves for thorium. See caption to Fig. 3.

does not apply, however, to the eight rare metals (In, Pd, Rh, Pt, Ta, Tl, Nb, Zr) at the bottom of Table I, the probable errors for which are approximately 3% in compression.

Previously reported[1] Hugoniot curves for 24ST aluminum, copper, and zinc are in substantial agreement with the present results. The present low-pressure (195-kilobar) zinc curve, however, indicates a 4% smaller compression than the previously drawn curve (Table III of reference 1). Similar comparisons of remaining data show agreement to 2% or better.

Present results may also be compared with shock-wave data obtained by another Los Alamos group using an electrical pin-contactor method.[2] The agreement with their tabulated "recent data" (24ST aluminum data sufficient to determine the Hugoniot curve from 145 to 330 kilobars) is everywhere better than 1% in compression, and is sufficiently good to indicate freedom from sizable consistent error of either method.

Impurities for the elements studied were determined by spectrochemical analysis. Specimens whose impurities exceeded 0.2% are: cobalt (0.5% Ni, 0.05% miscellaneous), nickel (0.1% Co, 0.05% each Mg, Si, Mn, Fe), titanium (0.05% each Al, Si, Cr, Mn, Sn).

The brass composition was 60.56% Cu, 39.31% zinc. The 24ST aluminum composition was 93.0% aluminum, 4.5% copper, 1.5% magnesium, 0.6% manganese.

F. Guide to Data Figures

The points below 100 kilobars, plotted as solid black disks in Figs. 3 to 29, are statically determined pressure-compression data taken from four articles by Bridgman.[5–8]

Except for the points around 400 kilobars, the iron

[6] P. W. Bridgman, Proc. Am. Acad. Arts Sci. **76**, 55 (1948).
[7] P. W. Bridgman, Proc. Am. Acad. Arts Sci. **76**, 9 (1945).
[8] P. W. Bridgman, Proc. Am. Acad. Arts Sci. **74**, 425 (1945).

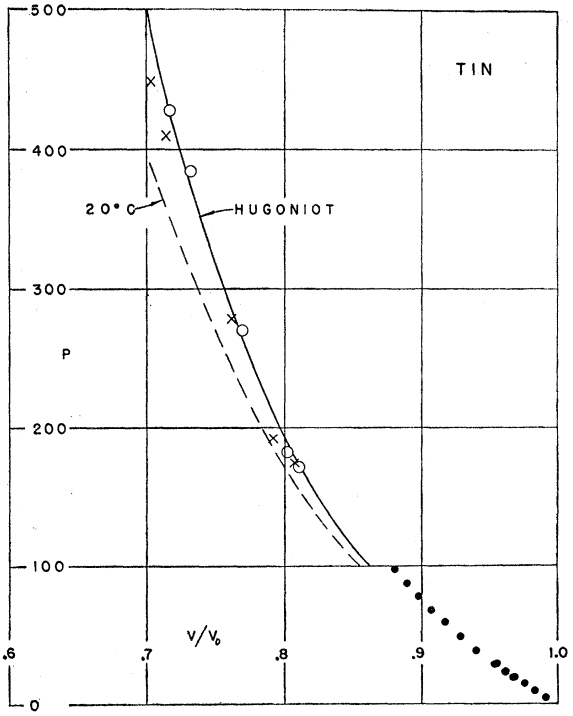

FIG. 17. Pressure-compression curves for tin. See caption to Fig. 3.

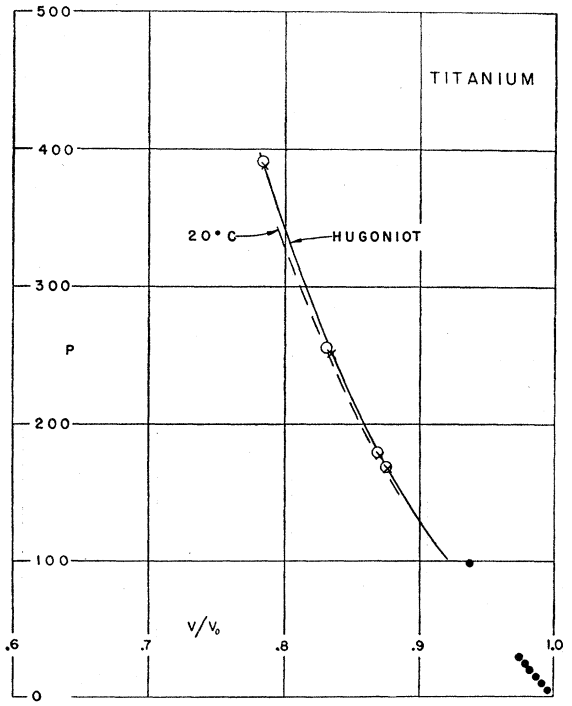

FIG. 18. Pressure-compression curves for titanium. See caption to Fig. 3.

data of Fig. 10 are reproduced from a recent article by Bancroft, Peterson, and Minshall.[9]

[9] Bancroft, Peterson, and Minshall, J. Appl. Phys. **27**, 291 (1956).

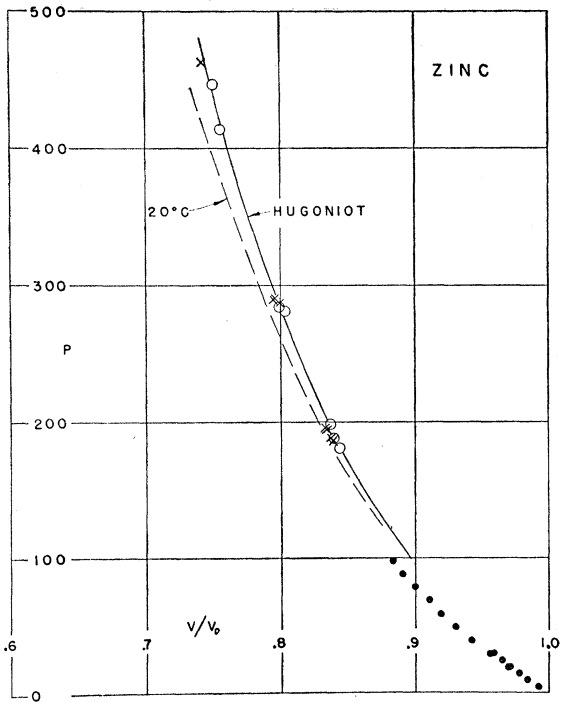

FIG. 19. Pressure-compression curves for zinc. See caption to Fig. 3.

II. EQUATION OF STATE

The purpose of the present section is to provide a complete thermodynamic description of all states neighboring the experimental Hugoniot curves. To this end, the Mie-Grüneisen equation of state is employed, for which the volume dependence of the Grüneisen ratio is determined using the Dugdale-MacDonald relation. These considerations lead to a complete P, V, E equation of state. This equation of state and available zero-pressure data then permit the calculation of remaining thermodynamic data of interest, and numerical results are tabulated for the various metals.

A. Theory

Mie-Grüneisen Equation of State

For the thermodynamic states of interest here, we shall assume that the thermal energy of a metallic crystal can be adequately described by means of a set of simple harmonic oscillators (the normal modes of the dynamical system) whose frequencies, ν_α, are functions only of volume. The internal energy, E, is then given by[10–12]

$$E=\Phi+\tfrac{1}{2}\sum_\alpha h\nu_\alpha+\sum_\alpha \frac{h\nu_\alpha}{e^{h\nu_\alpha/kT}-1}, \quad \alpha=1, \cdots 3N, \quad (8)$$

[10] See, for example, J. C. Slater, *Introduction to Chemical Physics* (McGraw-Hill Book Company, Inc., New York, 1939), Chap. XIII.

[11] F. Seitz, *Modern Theory of Solids* (McGraw-Hill Book Company, Inc., New York and London, 1940), Chap. III.

[12] M. Born and K. Huang, *Dynamical Theory of Crystal Lattices* (Clarendon Press, Oxford, 1954), Chap. II.

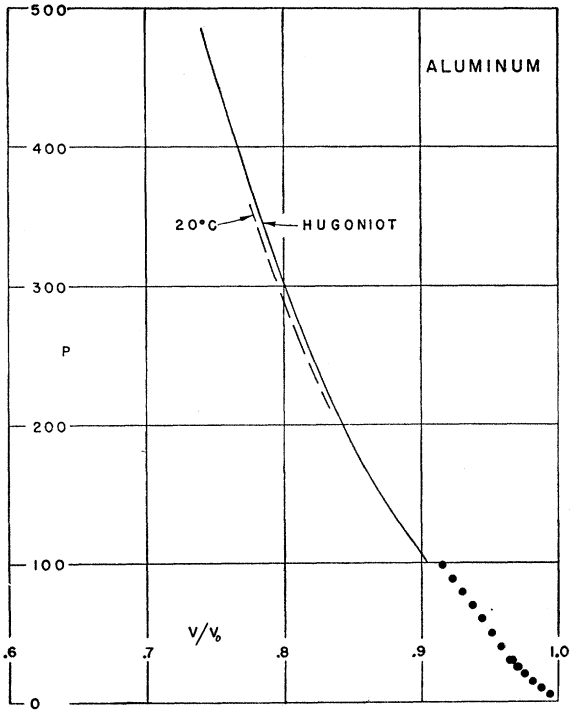

FIG. 20. Pressure-compression curves for 24ST aluminum. See caption to Fig. 3.

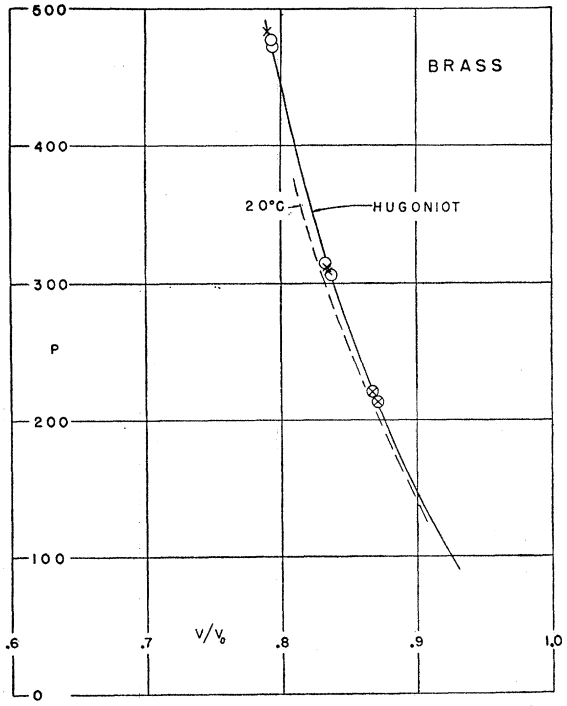

FIG. 21. Pressure-compression curves for brass. See caption to Fig. 3.

where Φ is the potential energy of the crystal with the particles at rest in their equilibrium positions, and the summation $(\sum_\alpha)$ is over the $3N$ normal modes of the crystal, N being the total number of atoms.

The pressure is given by

$$P=-\frac{d\Phi}{dV}+\frac{1}{V}\sum\gamma_\alpha\left\{\tfrac{1}{2}h\nu_\alpha+\frac{h\nu_\alpha}{e^{h\nu_\alpha/kT}-1}\right\}, \tag{9}$$

where

$$\gamma_\alpha=-d\ln\nu_\alpha/d\ln V. \tag{10}$$

Equation (9) simplifies in two interesting cases. If all the γ_α are equal (the consequences of simplifying assumptions discussed below), these quantities may be factored from the summation as γ. Alternatively, in the classical limit, the energies of all oscillators are equal, so that these quantities may be factored and γ becomes the average of the γ_α. In either case Eq. (9) reduces to the equation of state of Mie and Grüneisen,[13]

$$P=-\frac{d\Phi}{dV}+\frac{\gamma}{V}E_{\text{vib}}, \tag{11}$$

where E_{vib} is the vibrational contribution to the internal energy. A rearrangement of the terms in Eq. (11) yields

$$P+\left\{\frac{d\Phi}{dV}-\frac{\gamma}{V}\sum_\alpha\tfrac{1}{2}h\nu_\alpha\right\}=\frac{\gamma}{V}\sum_\alpha\frac{h\nu_\alpha}{e^{h\nu_\alpha/kT}-1} \tag{12a}$$

or

$$P-P_K=(\gamma/V)E_{\text{th}}=(\gamma/V)(E-E_K), \tag{12b}$$

[13] E. Grüneisen, *Handbuch der Physik* (Verlag J. Springer, Berlin, 1926), Vol. 10, p. 22.

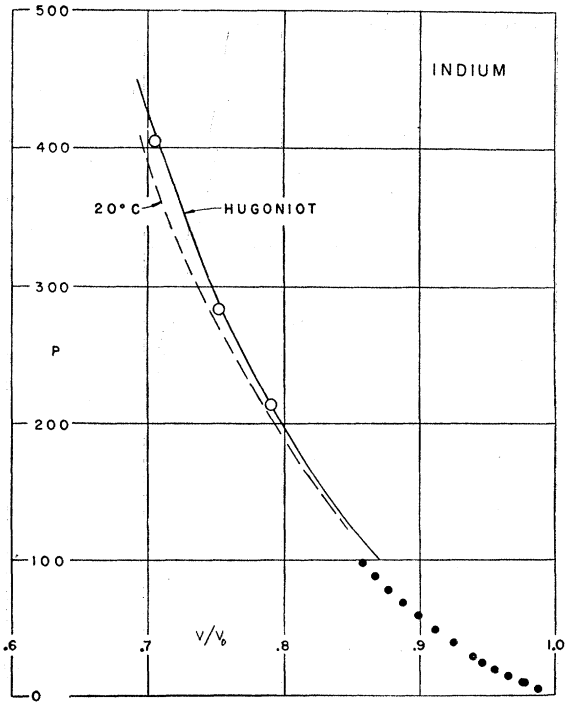

FIG. 22. Pressure-compression curves for indium. See caption to Fig. 3.

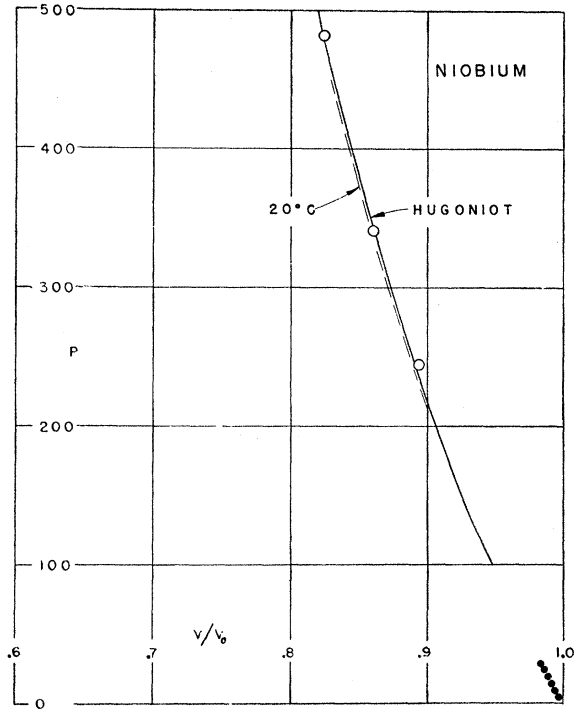

FIG. 23. Pressure-compression curves for niobium. See caption to Fig. 3.

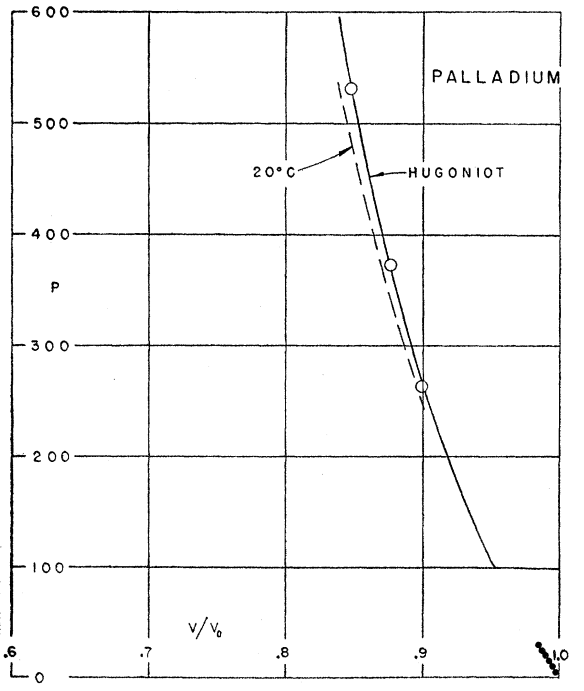

FIG. 24. Pressure-compression curves for palladium. See caption to Fig. 3.

where the subscript K refers to the quantities as a function of volume at 0°K. Grüneisen's ratio, γ, can be

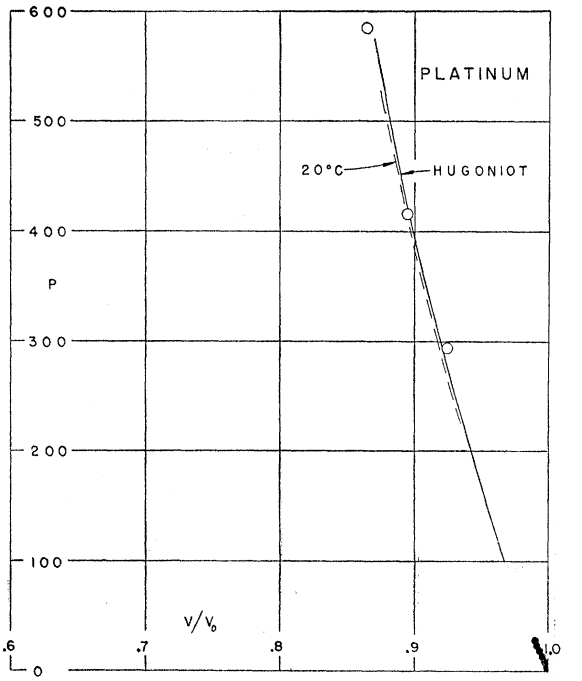

FIG. 25. Pressure-compression curves for platinum. See caption to Fig. 3.

expressed in terms of thermodynamic quantities by differentiating Eq. (12b). Since γ is a function only of volume,

$$\gamma = V\left(\frac{\partial P}{\partial E}\right)_V \equiv V\left(\frac{\partial P}{\partial T}\right)_V \Big/ C_v$$

$$\equiv -V\left(\frac{\partial P}{\partial V}\right)_T \left(\frac{\partial V}{\partial T}\right)_P \Big/ C_v$$

$$\equiv -V\left(\frac{\partial P}{\partial V}\right)_S \left(\frac{\partial V}{\partial T}\right)_P \Big/ C_p, \quad (13)$$

where C_v and C_p are the specific heats at constant volume and pressure, respectively. At zero pressure and room temperature γ can be evaluated from the measured values of the bulk modulus, thermal expansion coefficient, and specific heat; and for most metals the value so obtained lies between 1 and 3 (see Table III).

Equation (12b) can be rewritten in terms of any P, V, E curve, such as the experimental Hugoniot:

$$P - P_H = (\gamma/V)(E - E_H). \quad (14)$$

Determination below of the Grüneisen ratio $\gamma(V)$ then provides one with a complete P, V, E equation of state.

It is interesting to note, with respect to C_v, that the thermodynamic identity

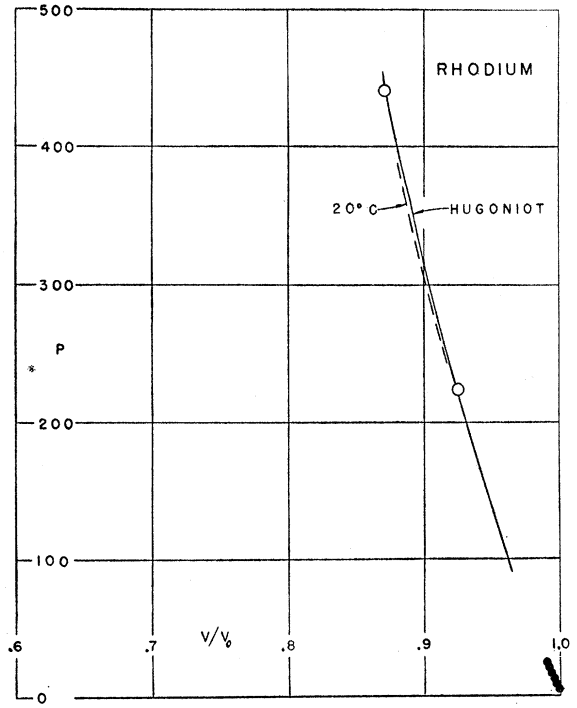

FIG. 26. Pressure-compression curves for rhodium. See caption to Fig. 3.

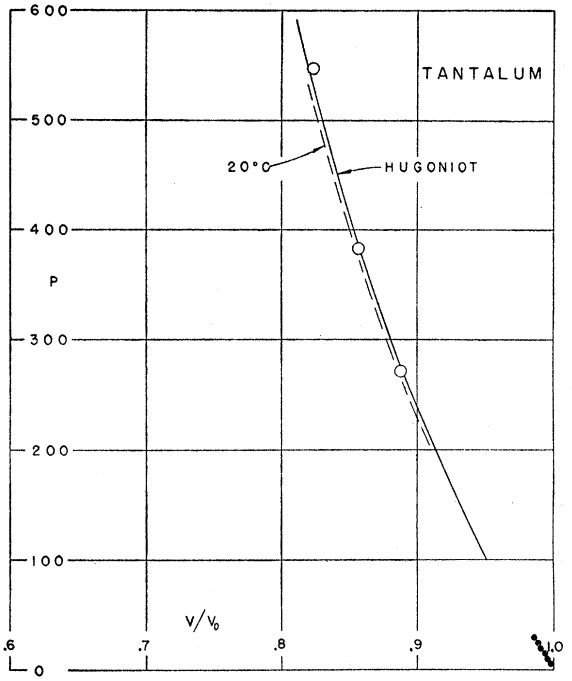

FIG. 27. Pressure-compression curves for tantalum. See caption to Fig. 3.

$$\left(\frac{\partial C_v}{\partial T}\right)_s = \frac{C_v}{T} + T\left(\frac{\partial P}{\partial T}\right)_v \left\{\frac{\partial}{\partial T}\left[\frac{C_v}{T(\partial P/\partial T)_v}\right]\right\}_v, \quad (15)$$

for γ a function only of volume, implies that C_v is a function only of entropy.

Grüneisen Ratio

Under the assumption that Poisson's ratio is independent of volume, Slater[14] extended the Debye theory for an isotropic continuum to obtain

$$\gamma = -\frac{V}{2}\left(\frac{d^2P/dV^2}{dP/dV}\right) - \tfrac{2}{3}. \quad (16)$$

Dugdale and MacDonald[15] proposed a modification of Slater's formula. Their result,

$$\gamma = -\frac{V}{2}\left(\frac{d^2(PV^{\frac{2}{3}})/dV^2}{d(PV^{\frac{2}{3}})/dV}\right) - \tfrac{1}{3}, \quad (17)$$

follows for cubic lattices from the assumption that all of the interatomic force constants change the same (percentagewise) upon compression of the lattice.[16]

Equations (16) and (17) differ by 0.33 at $P=0$, with Eq. (16) indicating the larger value. For most metal $P-V$ curves, the difference is less at higher pressure.

Quite recently, Barron[17,18] extended the Born-von Kármán theory to an essentially exact calculation of the Grüneisen ratio for a few simple lattice models. His results show that the γ_α are far from equal, though equality of the γ_α is implied by the simplifying assumptions used to establish either Eq. (16) or Eq. (17). In the classical limit (the calculations indicate $T \gtrsim 0.3\Theta$, where Θ is the Debye temperature), the Mie-Grüneisen equation of state is again valid. Comparisons of the γ obtained from Eq. (16) or Eq. (17) with the high-temperature results by Barron indicate fair agreement, with the Dugdale-MacDonald formula, Eq. (17), more nearly reproducing Barron's results. [For example, a model of the NaCl lattice gives $\gamma=2.3$ from Eq. (16), $\gamma=2.0$ from Eq. (17), while Barron's calculations indicate $\gamma=1.67$.]

At zero pressure, sufficient thermodynamic data exist to test the values of γ calculated from Eq. (16) or (17) against the thermodynamic values from Eq. (13). Slater[19,20] and Gilvarry,[21] using first and second derivatives of P obtained from Bridgman's data, have made extensive comparisons of the γ calculated from Eq. (16)

[14] Reference 10, p. 239.
[15] J. S. Dugdale and D. K. C. MacDonald, Phys. Rev. **89**, 832 (1953).
[16] Detailed in a forthcoming article "Compression of Solids by Strong Shock Waves" by Rice, McQueen, and Walsh, to appear in *Solid State Physics, Advances in Research and Application* (Academic Press, Inc., New York, 1957), Vol. VI. Zero-pressure tests of Eq. (17), results of which are summarized above, are also presented.
[17] T. H. K. Barron, Ann. Phys. **1**, 77 (1957).
[18] T. H. K. Barron, Phil. Mag. **46**, 720 (1955).
[19] J. C. Slater, reference 10, Chap. XXVII.
[20] J. C. Slater, Phys. Rev. **57**, 744 (1940).
[21] J. J. Gilvarry, Phys. Rev. **102**, 331 (1956).

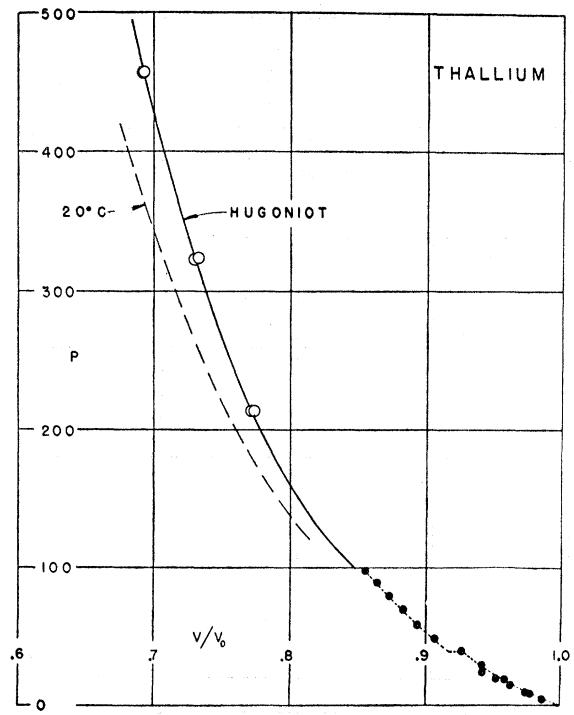

FIG. 28. Pressure-compression curves for thallium. See caption to Fig. 3.

with that from Eq. (13). For most metals the agreement is quite good. A similar comparison, using the present shock-wave data, has been carried out by the present authors.[16] Such a test is of interest because the shock wave results limit properly at zero pressure to the desired adiabatic first and second derivatives; also the extended data region of the present experimentation should lead to better precision in the determination of second derivatives of P. The tests, which show less scatter than the previous work, indicate somewhat more success for the Dugdale-MacDonald formula, Eq. (17), than for Eq. (16), though both are in substantial agreement with the experimental results. The former reproduces the values of γ from Eq. (13) with an average error of 15%.

In the following calculations, an attempt is made to obtain the most accurate description of high-pressure states. Accordingly, the experimental thermodynamic properties, i.e., of specific heats, thermal expansions, and γ_0, are employed along the zero-pressure isobars, and only the volume variation of γ is estimated by an empirical relation. The Dugdale-MacDonald formula, Eq. (17), is employed for this purpose. It is, of course, clear that the calculated values of γ, at high pressures, are not very accurate. In regard to calculated $P-V$ curves, on the other hand, γ is used only to estimate the small offsets (typically 1% in volume) from the experimental Hugoniot and errors as large as 25% in the offsets (i.e., approximately 25% in γ) lead to uncertainties which are only comparable to probable errors in the experimental curves. Temperature increases, calculated along constant-entropy curves, reflect an error which is roughly proportional to the volume-average error in γ. The use of the correct γ_0 at normal

TABLE III. Analytical fits of Grüneisen ratios. $\gamma=\gamma_0+A\mu+B\mu^2+C\mu^3$.

Metal	γ_0	A	B	C
Beryllium	1.17	−2.523	12.990	−31.851
Cadmium	2.27	13.417	−75.631	72.965
Chromium	1.08	10.965	−54.874	49.000
Cobalt	1.99	−5.906	26.354	−48.076
Copper	2.04	−3.296	10.493	−19.264
Gold	3.05	−21.876	115.18	−213.17
Lead	2.78	−8.406	22.791	−22.648
Magnesium	1.46	−2.078	4.621	−4.840
Molybdenum	1.58	−4.600	25.837	−61.398
Nickel	1.91	−8.007	35.275	−59.812
Silver	2.47	−5.670	19.334	32.891
Thorium	1.124	3.552	−14.223	15.552
Tin	2.03	9.4186	−52.133	66.016
Titanium	1.18	2.225	−9.904	11.052
Zinc	2.38	−6.087	18.626	−23.535
24ST aluminum	2.13	−7.245	24.707	−32.577
Brass	2.04	3.405	−26.304	38.692
Indium	2.238	−9.431	27.392	−26.186
Niobium	1.679	−5.882	26.261	−49.145
Palladium	2.183	26.824	−205.44	407.72
Platinum	2.627	−16.911	100.10	−216.84
Rhodium	2.265	−11.228	55.898	−109.85
Tantalum	1.689	−5.166	15.925	−18.991
Thallium	2.96	−3.617	2.264	−1.171
Zirconium	0.771	−0.449	0.285	−0.102

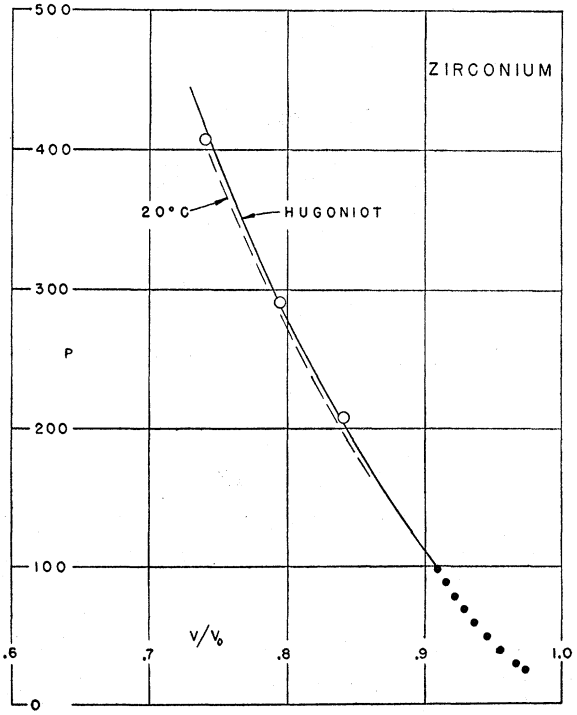

FIG. 29. Pressure-compression curves for zirconium. See caption to Fig. 3.

volume and an experimental additive term in the listed temperatures (T at $P=0$ on the adiabat through the point) then lead to temperatures which should be reliable to 10% or less of their centigrade values.

B. Calculations

Combining Eq. (17), which is assumed to be valid along the 0°K curve, with Eq. (14) yields the following equation for the pressure $P_K(V)$ at 0°K, in terms of the known Hugoniot curve, $P_H(V)$:

$$\frac{-\frac{1}{2}Vd^2(P_KV^{\frac{4}{3}})/dV^2}{d(P_KV^{\frac{4}{3}})/dV}-\frac{1}{3}=\frac{V(P_H-P_K)}{\frac{1}{2}P_H(V_{0H}-V)+E_{0H}+\int_{V_{0K}}^{V}PdV}. \quad (18)$$

The initial conditions required for the integration of Eq. (18) are the specific volume, the compressibility at 0°K, $P_K=0$, and the specific internal energy, E_{0H}, at the foot of the Hugoniot (relative to an arbitrary zero energy at $P=0$, $T=0$°K). These quantities were obtained from rough extrapolations[22] of available zero pressure data to 0°K. Zero-degree-Kelvin pressure-volume curves, obtained by numerical integration of Eq. (18), are listed in Table IV. Analytical fits of the associated $\gamma(V)$ curves, which may now be obtained from either Eq. (14) or Eq. (17). are given in Table III.

Differentiating Eq. (14) gives

$$P_A=-\frac{dE_H}{dV}+(P_H-P_A)\frac{d}{dV}\left(\frac{V}{\gamma}\right)+\frac{V}{\gamma}\left(\frac{dP_H}{dV}-\frac{dP_A}{dV}\right), \quad (19)$$

which is a first odrer differential equation for an adiabat, $P_A(V)$, in terms of the known $P_H(V)$, $E_H(V)$, and $\gamma(V)$. Equation (19) was integrated numerically to obtain serveral adiabats for each metal. Two of these, the adiabat which coincides with the foot of the Hugoniot and an adiabat which intersects the Hugoniot curve at a pressure near the upper limit of the experimental data, are listed in Table IV.

At constant entropy the thermodynamic identity

$$TdS=C_vdT+T(\partial P/\partial T)_VdV=0$$

can be integrated to give temperature as a function of volume:

$$T=T_i\exp\left[-\int_{V_i}^{V}\frac{\gamma}{V}dV\right]. \quad (20)$$

Here the relation $\gamma=V(\partial P/\partial T)_V/C_v$ was used, and T_i is an initial temperature at some volume V_i on the adiabat. Values of T_i, V_i were obtained along $P=0$ from available thermal expansion data. Equation (20) can then be used together with the adiabatic P-V curves determined above to obtain the temperature at any P-V point neighboring the Hugoniot curve. Resulting temperatures for pressure-volume points along two adiabats are listed in Table IV. Temperatures along the Hugoniot curve for each metal are also listed in Table IV and the 20°C isotherms are plotted in Figs. 3–29.

Calculated values of the ratio

$$\frac{U_r}{U_p}=\int_0^{PH}(-dV/dP_A)^{\frac{1}{2}}dP_A\Big/[P_H(V_{0H}-V)]^{\frac{1}{2}} \quad (21)$$

(see Eq. 4 and associated discussion) are listed in Table V for the various solids. The denominator in Eq. (21) is the expression for the shock wave particle velocity corresponding to shock pressure P_H and is a consequence of Eqs. (1) and (2). The numerator[23] is the Reimann integral for the particle velocity due to the centered, simple rarefaction wave which relieves the pressure from P_H to zero, and is evaluated using the adiabat which intersects the Hugoniot curve at P_H. The refinements indicated by the present calculations cause a slight shift of the P, V points, plotted as ×'s in the figures, which were obtained by using Eq. (4). The corrections reduce the compression offsets (between the ×'s and the curves drawn through the graphical solutions) from an average magnitude of 1.1% to 0.7%.

It should be noted that three metals, lead, tin and cadmium, exhibit free-surface-approximation solutions which are in sizable disagreement with results obtained from the graphical solutions. The three are all low-melting-point metals and are, indeed, the only metals (among those for which free-surface velocity measure-

[22] The values of E_{0H} were obtained by integrating the Debye specific heat curve. Values of the initial volume, V_{0K}, were those which satisfied Eq. (14) evaluated at $V=V_{0K}$:

$$[\gamma_{0H}+(d\gamma/dV)_{0H}(V_{0H}-V_{0K})][E_{0H}+\tfrac{1}{2}P_H(V_{0H}-V_{0K})]=V_{0K}P_H,$$

where the first bracket is an approximate value for γ at V_{0K}. The compressibility at 0°K, $P_K=0$, was obtained from the derivative of Eq. (14) evaluated at $V=V_{0K}$:

$$V_{0K}(dP_K/dV)_{V=V_{0K}}=[P_H-E_H(d\gamma/dV)-\gamma(dE_H/dV)]_{V=V_{0K}}.$$

Approximate values of $d\gamma/dV$, necessary for the evaluation of each of the above relations, were obtained from Eq. (17), and the assumption that the right side of Eq. (17) can be determined using the adiabat through the foot of the Hugoniot curve. Consequent values of γ_0 and $d\gamma/dV$ are

$$\gamma_{0H}=B/A,$$

$$V_{0H}\left(\frac{d\gamma}{dV}\right)_{0H}=\frac{5}{2}\frac{B^2}{A^2}-\frac{7}{6}\frac{B}{A}-3\frac{C}{A}-\frac{1}{9}.$$

The first of these relations was also used in Sec. I to determine the values of B/A used in analytical fits of the experimental data.

[23] See, for example, R. Courant and K. O. Friedricks, *Supersonic Flow and Shock Waves* (Interscience Publishers, Inc., New York, 1948). The present expression can be obtained from their Eq. (34.05).

TABLE IV. Pressure-volume loci and associated temperatures (degrees centigrade). The first adiabat listed for each material coincides with the Hugoniot curve at 20°C, zero pressure. The second adiabat intersects the Hugoniot curve near the high-pressure limit of the experimental data. The pressure at which the second adiabat crosses the Hugoniot curve is given in parentheses.

$\backslash P$(kilobars)	0	100	150	200	250	300	350	400	450	500
Beryllium										
0°K	0.9982	0.9263	0.8972	0.8716	0.8487	0.8275	0.8082			
Hugoniot	1.000	0.9277	0.8990	0.8725	0.8503	0.8299	0.8110			
T_H	20°C	50°	70°	97°	127°	168°	213°			
Adiabat	1.000	0.9276	0.8987	0.8728	0.8493	0.8284				
T_A	20°C	45	55	64	74	82				
Adiabat (309 kilobars)	1.003	0.9301	0.9010	0.8742	0.8506	0.8299	0.8103			
T_A	97°C	129	143	155	164	181	187			
Cadmium										
0°K	0.9764	0.8524	0.8188	0.7932	0.7716	0.7527	0.7364	0.7220	0.7093	0.6972
Hugoniot	1.000	0.8742	0.8403	0.8141	0.7932	0.7752	0.7597	0.7464	0.7345	0.7237
T_H	20°C	210	349	515	697	895	1111	1335	1563	1800
Adiabat	1.000	0.8708	0.8339	0.8050	0.7819	0.7620	0.7450	0.7300	0.7164	0.7041
T_A	20°C	157	213	257	297	331	359	384	408	431
Adiabat (318 kilobars)	1.028	0.8976	0.8568	0.8244	0.7982	0.7763	0.7573	0.7414	0.7265	0.7136
T_A	310°C	559	674	784	866	945	1014	1072	1125	1177
Chromium										
0°K	0.9969	0.9528	0.9336	0.9160	0.9006	0.8860	0.8730	0.8607	0.8492	0.8387
Hugoniot	1.000	0.9561	0.9373	0.9202	0.9050	0.8908	0.8779	0.8658	0.8548	0.8447
T_H	20°C	39	54	73	96	126	161	199	242	291
Adiabat	1.000	0.9561	0.9372	0.9201	0.9044	0.8899	0.8717	0.8642	0.8529	0.8421
T_A	20°C	37	46	56	66	76	86	95	103	112
Adiabat (522 kilobars)	1.003	0.9595	0.9410	0.9238	0.9081	0.8933	0.8798	0.8674	0.8560	0.8449
T_A	170°C	194	209	223	238	253	267	281	295	307
Cobalt										
0°K	0.9931	0.9500	0.9318	0.9150	0.9000	0.8863	0.8734	0.8112	0.8500	0.8395
Hugoniot	1.000	0.9552	0.9368	0.9200	0.9050	0.8915	0.8782	0.8160	0.8551	0.8450
T_H	20°C	48	65	86	109	134	166	202	241	283
Adiabat	1.000	0.9552	0.9366	0.9197	0.9045	0.8905	0.8770	0.8145	0.8531	0.8422
T_A	20°C	45	57	67	76	86	96	104	111	117
Adiabat (523 kilobars)	1.005	0.9581	0.9392	0.9221	0.9065	0.8926	0.8792	0.8165	0.8551	0.8447
T_A	120°C	155	171	185	199	211	224	235	245	254
Copper										
0°K	0.9903	0.9337	0.9109	0.8908	0.8732	0.8571	0.8424	0.8290	0.8165	0.8049
Hugoniot	1.000	0.9412	0.9186	0.8980	0.8803	0.8643	0.8500	0.8370	0.8249	0.8137
T_H	20°C	63	89	121	158	201	255	311	373	444
Adiabat	1.000	0.9408	0.9180	0.8974	0.8781	0.8625	0.8472	0.8334	0.8209	0.8092
T_A	20°C	57	73	85	99	111	123	134	145	155
Adiabat (504 kilobars)	1.010	0.9490	0.9255	0.9038	0.8852	0.8683	0.8528	0.8387	0.8255	0.8143
T_A	215°C	279	306	331	353	375	395	415	432	448
Gold										
0°K	0.9900	0.9458	0.9277	0.9113	0.8966	0.8829	0.8707	0.8589	0.8480	0.8377
Hugoniot	1.000	0.9521	0.9334	0.9167	0.9018	0.8882	0.8759	0.8643	0.8537	0.8438
T_H	20°C	65	96	121	153	200	253	311	372	443
Adiabat	1.000	0.9520	0.9331	0.9161	0.9014	0.8874	0.8744	0.8626	0.8514	0.8412
T_A	20°C	59	74	86	97	108	117	125	133	141
Adiabat (518 kilobars)	1.009	0.9583	0.9382	0.9210	0.9053	0.8910	0.8779	0.8660	0.8546	0.8441
T_A	235°C	311	338	361	383	401	419	434	449	464
Lead										
0°K	0.9762	0.8492	0.8113	0.7808	0.7558	0.7340	0.7150	0.6979	0.6829	0.6690
Hugoniot	1.000	0.8623	0.8253	0.7958	0.7722	0.7523	0.7348	0.7191	0.7051	0.6930
T_H	20°C	228	375	609	861	1150	1459	1812	2192	2575
Adiabat	1.000	0.8600	0.8203	0.7888	0.7628	0.7403	0.7206	0.7034	0.6878	0.6736
T_A	20°C	139	179	210	241	267	289	310	329	360
Adiabat (204 kilobars)	1.020	0.8695	0.8288	0.7959	0.7696	0.7465	0.7266	0.7585	0.7426	0.7280
T_A	249°C	485	563	624	682	730	773	814	854	891

TABLE IV.—*Continued.*

$\backslash P$ (kilobars)	0	100	150	200	250	300	350	400	450	500
Magnesium										
0°K	0.9985	0.8200	0.7604	0.7304	0.6980	0.6699				
Hugoniot	1.000	0.8300	0.7712	0.7432	0.7123	0.6861				
T_H	20°C	174	313	487	691	923				
Adiabat	1.000	0.8278	0.7670	0.7362	0.7032	0.6737				
T_A	20°C	74	131	155	176	196				
Adiabat (229 kilobars)	1.023	0.8395	0.7769	0.7450	0.7110	0.6816				
T_A	296°C	447	526	576	620	660				
Molybdenum										
0°K	0.9971	0.9636	0.9486	0.9347	0.9219	0.9096	0.8979	0.8870	0.8768	0.8670
Hugoniot	1.000	0.9660	0.9510	0.9369	0.9240	0.9119	0.9002	0.8895	0.8794	0.8698
T_H	20°C	37	49	62	79	101	125	154	188	227
Adiabat	1.000	0.9659	0.9508	0.9368	0.9239	0.9117	0.8999	0.8890	0.8786	0.8685
T_A	20°C	35	43	49	55	61	67	72	77	83
Adiabat (500 kilobars)	1.002	0.9674	0.9522	0.9382	0.9250	0.9128	0.9011	0.8900	0.8799	0.8696
T_A	139°C	161	171	180	189	197	205	213	221	228
Nickel										
0°K	0.9930	0.9551	0.9320	0.9151	0.8999	0.8855	0.8720	0.8599	0.8480	0.8370
Hugoniot	1.000	0.9501	0.9367	0.9197	0.9042	0.8900	0.8769	0.8643	0.8530	0.8422
T_H	20°C	43	61	79	101	125	150	181	217	254
Adiabat	1.000	0.9500	0.9364	0.9195	0.9038	0.8890	0.8758	0.8633	0.8517	0.8401
T_A	20°C	43	54	63	71	79	86	93	100	106
Adiabat (508 kilobars)	1.005	0.9588	0.9397	0.9220	0.9062	0.8918	0.8781	0.8653	0.8536	0.8423
T_A	136°C	171	186	199	210	221	231	241	251	259
Silver										
0°K	0.9878	0.9202	0.8951	0.8734	0.8547	0.8380	0.8229	0.8090	0.7960	0.7833
Hugoniot	1.000	0.9291	0.9037	0.8818	0.8632	0.8470	0.8322	0.8190	0.8066	0.7953
T_H	20°C	88	130	186	255	326	417	520	627	747
Adiabat	1.000	0.9286	0.9028	0.8804	0.8612	0.8437	0.8279	0.8138	0.8006	0.7886
T_A	20°C	74	96	114	131	148	168	176	189	201
Adiabat (479 kilobars)	1.017	0.9406	0.9133	0.8900	0.8697	0.8520	0.8353	0.8207	0.8074	0.7980
T_A	314°C	433	483	524	560	594	627	656	682	708
Thorium										
0°K	0.9920	0.8643	0.8222	0.7878	0.7594	0.7348	0.7128	0.6939	0.6767	0.6610
Hugoniot	1.000	0.8727	0.8310	0.7979	0.7705	0.7473	0.7274	0.7099	0.6943	0.6806
T_H	20°C	122	227	377	552	752	969	1197	1419	1631
Adiabat	1.000	0.8716	0.8283	0.7938	0.7647	0.7396	0.7176	0.6979	0.6802	0.6634
T_A	20°C	76	101	124	145	164	181	197	212	225
Adiabat (483 kilobars)	1.035	0.8989	0.8540	0.8163	0.7856	0.7586	0.7352	0.7146	0.6960	0.6784
T_A	802°C	1003	1095	1183	1263	1339	1405	1467	1525	1581
Tin										
0°K	0.9806	0.8439	0.8068	0.7778	0.7540	0.7334	0.7159	0.7002		
Hugoniot	1.000	0.8614	0.8248	0.7964	0.7735	0.7544	0.7382	0.7240		
T_H	20°C	219	377	556	752	953	1139	1318		
Adiabat	1.000	0.8580	0.8183	0.7877	0.7622	0.7414	0.7229	0.7062		
T_A	20°C	149	198	239	275	305	332	358		
Adiabat (205 kilobars)	1.012	0.8710	0.8297	0.7970	0.7703	0.7479	0.7289	0.7120		
T_A	208°C	415	497	569	631	683	731	773		
Titanium										
0°K	0.9944	0.9119	0.8801	0.8527	0.8290	0.8077	0.7888	0.7713		
Hugoniot	1.000	0.9170	0.8857	0.8587	0.8354	0.8148	0.7964	0.7809		
T_H	20°C	65	105	155	223	302	394	491		
Adiabat	1.000	0.9168	0.8851	0.8576	0.8334	0.8118	0.7921	0.7730		
T_A	20°C	54	70	84	97	111	123	135		
Adiabat (340 kilobars)	1.005	0.7222	0.8898	0.8618	0.8375	0.8155	0.7963	0.7776		
T_A	210°C	266	290	314	337	359	380	400		

TABLE IV.—*Continued.*

$\backslash P$ (kilobars)	0	100	150	200	250	300	350	400	450	500
Zinc										
0°K	0.9800	0.8834	0.8507	0.8234	0.8004	0.7802	0.7622	0.7458	0.7310	0.7180
Hugoniot	1.000	0.8960	0.8633	0.8363	0.8140	0.7942	0.7767	0.7615	0.7482	0.7360
T_H	20°C	119	187	272	369	482	609	747	900	1061
Adiabat	1.000	0.8949	0.8608	0.8328	0.8082	0.7875	0.7690	0.7522	0.7371	0.7232
T_A	20°C	96	123	147	169	189	207	224	239	254
Adiabat (404 kilobars)	1.030	0.9126	0.8760	0.8456	0.8208	0.7985	0.7792	0.7619	0.7460	0.7318
T_A	302°C	479	540	593	641	681	720	756	791	821
Aluminum										
0°K	0.9874	0.8966	0.8641	0.8362	0.8126	0.7915	0.7724	0.7553	0.7400	0.7255
Hugoniot	1.000	0.9045	0.8716	0.8441	0.8210	0.8008	0.7824	0.7661	0.7513	0.7380
T_H	20°C	94	153	223	308	405	518	637	770	909
Adiabat	1.000	0.9036	0.8701	0.8422	0.8180	0.7961	0.7770	0.7594	0.7435	0.7288
T_A	20°C	78	100	119	135	150	163	177	189	201
Adiabat (513 kilobars)	1.034	0.9250	0.8886	0.8578	0.8319	0.8092	0.7892	0.7710	0.7543	0.7392
T_A	454°C	633	703	755	799	841	881	915	949	981
Brass										
0°K	0.9869	0.9140	0.8876	0.8649	0.8453	0.8283	0.8130	0.7990	0.7864	0.7745
Hugoniot	1.000	0.9250	0.8984	0.8758	0.8564	0.8395	0.8250	0.8115	0.7992	0.7882
T_H	20°C	89	129	175	235	305	382	467	557	651
Adiabat	1.000	0.9244	0.8971	0.8739	0.8538	0.8360	0.8200	0.8056	0.7922	0.7803
T_A	20°C	73	96	118	137	155	171	187	201	215
Adiabat (446 kilobars)	1.014	0.9363	0.9081	0.8839	0.8620	0.8442	0.8277	0.8129	0.7991	0.7860
T_A	230°C	323	363	401	436	468	499	527	552	577
Indium										
0°K	0.9801	0.8604	0.8210	0.7880	0.7600	0.7351	0.7135	0.6943	0.6769	0.6610
Hugoniot	1.000	0.8701	0.8302	0.7979	0.7710	0.7478	0.7270	0.7087	0.6922	0.6774
T_H	20°C	153	260	397	561	745	950	1179	1439	1710
Adiabat	1.000	0.8687	0.8276	0.7939	0.7650	0.7400	0.7180	0.6983	0.6800	0.6624
T_A	20°C	99	124	144	163	181	195	210	223	233
Adiabat (474 kilobars)	1.002	0.8969	0.8507	0.8142	0.7833	0.7566	0.7336	0.7124	0.6936	0.6760
T_A		1055°C	1157	1242	1314	1381	1439	1495	1547	1593
Niobium										
0°K	0.9951	0.9440	0.9226	0.9032	0.8856	0.8694	0.8544	0.8404	0.8271	0.8148
Hugoniot	1.000	0.9476	0.9260	0.9067	0.8894	0.8730	0.8582	0.8449	0.8321	0.8197
T_H	20°C	49	73	97	133	177	227	284	351	427
Adiabat	1.000	0.9475	0.9256	0.9061	0.8885	0.8721	0.8566	0.8427	0.8296	0.8171
T_A	20°C	45	55	65	73	81	89	96	103	110
Adiabat (528 kilobars)	1.006	0.9526	0.9302	0.9104	0.8923	0.8756	0.8601	0.8459	0.8326	0.8200
T_A	287°C	335	358	377	393	409	424	439	452	465
Palladium										
0°K	0.9918	0.9422	0.9233	0.9071	0.8930	0.8808	0.8696	0.8596	0.8500	0.8410
Hugoniot	1.000	0.9520	0.9330	0.9170	0.9029	0.8903	0.8792	0.8692	0.8600	0.8513
T_H	20°C	65	97	135	180	231	289	353	423	497
Adiabat	1.000	0.9517	0.9326	0.9159	0.9011	0.8882	0.8766	0.8658	0.8556	0.8466
T_A	20°C	61	79	104	125	143	159	177	192	205
Adiabat (481 kilobars)	1.006	0.9587	0.9399	0.9230	0.9080	0.8941	0.8820	0.8710	0.8609	0.8512
T_A	187°C	246	278	311	343	375	403	429	454	477
Platinum										
0°K	0.9940	0.9632	0.9500	0.9377	0.9260	0.9154	0.9052	0.8959	0.8868	0.8779
Hugoniot	1.000	0.9679	0.9540	0.9412	0.9298	0.9190	0.9087	0.8993	0.8903	0.8819
T_H	20°C	46	60	77	95	117	144	174	207	244
Adiabat	1.000	0.9678	0.9539	0.9410	0.9292	0.9183	0.9081	0.8985	0.8891	0.8806
T_A	20°C	44	54	63	71	78	85	91	97	102
Adiabat (481 kilobars)	1.003	0.9697	0.9567	0.9429	0.9310	0.9199	0.9096	0.8999	0.8905	0.8819
T_A	119°C	151	165	177	187	197	207	216	224	231

TABLE IV.—*Continued.*

$\backslash P$(kilobars)	0	100	150	200	250	300	350	400	450	500
Rhodium										
0°K	0.9946	0.9642	0.9509	0.9380	0.9264	0.9156	0.9053	0.8958	0.8864	0.8778
Hugoniot	1.000	0.9683	0.9548	0.9419	0.9301	0.9191	0.9090	0.8992	0.8899	0.8812
T_H	20°C	42	54	69	85	104	127	153	181	218
Adiabat	1.000	0.9683	0.9545	0.9417	0.9299	0.9188	0.9081	0.8982	0.8889	0.8802
T_A	20°C	41	48	56	64	71	77	83	89	97
Adiabat (478 kilobars)	1.002	0.9698	0.9561	0.9432	0.9311	0.9200	0.9095	0.8998	0.8901	0.8811
T_A	106°C	133	144	155	165	173	181	189	197	204
Tantalum										
0°K	0.9952	0.9463	0.9273	0.9089	0.8921	0.8768	0.8622	0.8489	0.8363	0.8244
Hugoniot	1.000	0.9510	0.9307	0.9122	0.8955	0.8803	0.8657	0.8524	0.8400	0.8284
T_H	20°C	47	69	92	121	160	207	260	315	379
Adiabat	1.000	0.9510	0.9304	0.9119	0.8951	0.8795	0.8649	0.8510	0.8383	0.8264
T_A	20°C	45	55	61	70	79	86	93	99	106
Adiabat (540 kilobars)	1.005	0.9555	0.9345	0.9156	0.8983	0.8827	0.8680	0.8539	0.8411	0.8290
T_A	272°C	314	336	354	369	383	397	410	423	435
Thallium										
0°K	0.8446	0.8229	0.7850	0.7558	0.7314	0.7117	0.6937	0.6782	0.6642	0.6510
Hugoniot	1.000	0.8440	0.8063	0.7785	0.7558	0.7368	0.7203	0.7063	0.6940	0.6822
T_H	20°C	315	531	791	1079	1392	1719	2105	2447	2831
Adiabat	1.000	0.8387	0.7987	0.7672	0.7416	0.7200	0.7016	0.6849	0.6708	0.6578
T_A	20°C	192	248	293	333	367	398	425	450	473
Adiabat (489 kilobars)	1.097	0.9072	0.8542	0.8142	0.7822	0.7557	0.7335	0.7141	0.6969	0.6817
T_A	671°C	1383	1656	1181	2076	2247	2401	2534	2657	2769
Zironium										
0°K	0.9968	0.9068	0.8709	0.8394	0.8112	0.7860	0.7629	0.7420	0.7227	0.7049
Hugoniot	1.000	0.9098	0.8739	0.8421	0.8144	0.7894	0.7670	0.7467	0.7280	0.7104
T_H	20°C	55	92	143	214	298	395	503	616	737
Adiabat	1.000	0.9090	0.8733	0.8414	0.8131	0.7879	0.7646	0.7435	0.7244	0.7062
T_A	20°C	41	50	59	67	75	81	88	94	99
Adiabat (459 kilobars)	1.008	0.9159	0.8792	0.8470	0.8182	0.7925	0.7690	0.7480	0.7281	0.7100
T_A	447°C	502	526	547	565	584	601	618	633	647

ments were made) for which the calculations indicate melting in the present experimental range. Shock waves just strong enough for incipient melting of lead, tin, and cadmium (initially at 20°C) are 245 kilobars, 225 kilobars, and 325 kilobars, respectively. For stronger shock waves, at least partial melting occurs as the material is relieved to zero pressure. Melting phenomena are not included in any of the calculations of the present paper.

24ST aluminum data for hydrodynamic applications are listed in Tables VI and VII. The calculations were carried out by the methods outlined above and did incorporate the refinement of the free-surface velocity approximation.

SUMMARIZING REMARKS

Shock-wave experiments were performed to determine Hugoniot curves to pressures of several hundred kilobars. The Hugoniot curves, the Mie-Grüneisen equation of state, and the Dugdale-MacDonald formula were then employed to calculate complete thermodynamic descriptions of the various metals, for states neighboring the experimental curves. The calculated offsets between the Hugoniot curves and neighboring $P-V$

TABLE V. Ratio of the Riemann integral to the shock wave particle velocity, as a function of shock pressure.

Metal	100 kilobars	300 kilobars	500 kilobars
Beryllium	1.000	1.003	
Cadmium	1.005	1.031	melting
Chromium	1.000	1.000	1.001
Cobalt	1.000	1.003	1.008
Copper	1.001	1.005	1.012
Gold	1.000	1.006	1.016
Lead	1.009	melting	melting
Magnesium	1.005	1.027	
Molybdenum	1.000	1.001	1.002
Nickel	1.000	1.003	1.007
Silver	1.002	1.011	1.024
Thorium	1.001	1.010	1.022
Tin	1.003	melting	melting
Titanium	1.000	1.002	1.006
Zinc	1.004	1.022	1.042
24ST aluminum	1.003	1.015	1.030
Brass	1.001	1.009	1.019
Indium	1.008	melting	melting
Niobium	1.000	1.003	1.007
Palladium	1.000	1.004	1.009
Platinum	1.001	1.003	1.006
Rhodium	1.000	1.002	1.005
Tantalum	1.000	1.002	1.005
Thallium	1.014	melting	melting
Zirconium	1.000	1.001	1.003

TABLE VI. Shock wave parameters for 24ST aluminum.

Shock wave pressure P (kilobars)	Relative volume V/V_0	Shock wave velocity U_s km/sec	Shock particle velocity U_p km/sec	Sound speed C km/sec	Temperature T °C
100	0.9043	6.125	0.571	6.307	99
125	0.8873	6.305	0.712	6.497	125
150	0.8716	6.475	0.831	6.667	154
175	0.8573	6.640	0.947	6.825	187
200	0.8441	6.793	1.057	6.970	223
225	0.8322	6.940	1.165	7.106	264
250	0.8210	7.082	1.267	7.233	308
275	0.8104	7.220	1.368	7.348	356
300	0.8008	7.350	1.465	7.465	406
325	0.7912	7.476	1.561	7.624	460
350	0.7824	7.598	1.654	7.675	516
375	0.7740	7.718	1.744	7.771	576
400	0.7661	7.836	1.832	7.862	637
425	0.7585	7.950	1.920	7.948	702
450	0.7513	8.062	2.003	8.032	768
475	0.7445	8.171	2.082	8.112	837
500	0.7380	8.276	2.170	8.190	907

curves of interest are generally small, only a few percent in compression. Hence, despite the approximations inherent in the Mie-Grüneisen and Dugdale-MacDonald equations, errors arising in the $P-V$ curves due to the calculations are probably only comparable to uncertainties in the experimental data.

The important question of equivalence for the shock-wave results and laboratory pressure-volume data is perhaps best evaluated by examination of the data plots, Figs. 3 to 29. For most metals, the compatibility, if judged by downward extrapolation of the analytical fits, is quite good. This is especially true of comparisons

TABLE VII. Pressure *versus* particle velocity curves for 24ST aluminum. Each number in parentheses is a particle velocity (km/sec) for the corresponding shock pressure (kilobars). Remaining numbers in a given column then trace out the associated cross curve (see Fig. 2 and Section IB).

P	Particle velocity								
0	1.165	1.655	2.098	2.576	2.945	3.380	3.680	...	...
100	(0.571)	1.075	1.775	1.960	2.345	2.750	3.082	3.445	...
150	0.342	(0.831)	1.285	1.707	2.100	2.493	2.833	3.188	3.613
200	0.118	0.606	(1.057)	1.480	1.875	2.260	2.605	2.958	3.375
250	...	0.400	0.848	(1.267)	1.662	2.042	2.394	2.744	3.130
300	...	0.203	0.652	1.066	(1.465)	1.844	2.195	2.543	2.950
350	...	0.008	0.465	0.880	1.280	(1.654)	2.010	2.352	2.688
400	...	...	0.290	0.700	1.107	1.473	(1.832)	2.177	2.507
450	...	...	0.120	0.527	0.935	1.302	1.662	(2.003)	2.337
500	...	...	...	0.364	0.765	1.136	1.500	1.838	(2.170)

with the recent measurements to 30 kilobars by Professor Bridgman. Several of the static measurements to 100 kilobars, however, indicate compressions which are a few percent smaller than the corresponding shock wave results. In regard to the latter comparisons, it should be noted that the approximate nature of either of the present basic assumptions (thermal equilibrium and isotropy) would cause the shock wave results to indicate too little compression, and hence is not in the desired direction to account for the small observed offsets.

ACKNOWLEDGMENTS

The present effort was made possible only through the cooperation of a large number of people, most of whom are members of the GMX Division of the Los Alamos Scientific Laboratory.